CHARACTERIZATION OF THE 1966 CAMP CENTURY SUBGLACIAL
SEDIMENT CORE: A MULTISCALE ANALYSIS

A Thesis Presented

by

Cat Collins

to

The Faculty of the Graduate College

of

The University of Vermont
In Partial Fulfillment of the Requirements
for the Degree of Master of Science
Specializing in Natural Resources

August, 2024

Defense Date: May 3, 2024
Thesis Examination Committee:

Paul Bierman Ph. D, Advisor
Donna Rizzo Ph. D, Chairperson
Nico Perdrial, Ph.D.
Holger Hoock, D. Phil, Dean of the Graduate College

ABSTRACT

In 1966, drilling at Camp Century recovered 3.44 meters of subglacial material from beneath 1350 meters of ice. While prior analysis of this subglacial material showed that the core includes glacial sediment, ice, and sediment deposited during an interglacial, it had never been thoroughly studied. To better characterize this material, we analyzed 26 of the 30 samples remaining in the archive. We performed a multi-scale analysis including X-ray diffraction, micro-computed tomography, and scanning electron microscopy to delineate stratigraphic units and assign facies based on inferred depositional processes.

At the macro-scale, quantitative X-ray diffraction revealed quartz and feldspar dominance and little variation in relative mineral abundance between samples. Meso-scale evaluation of the frozen sediments using micro-computed tomography scans showed clear variations in the stratigraphy of the core characterized by the presence of layering, grading, and sorting structures. Micro-scale grain size and shape analysis, conducted using scanning electron microscopy, showed an abundance of fine-grained materials in the lower portion of the core and no correlation between grain shape parameters and depth. These multiscale data define 5 distinct stratigraphic units within the core based on sedimentary process and K-means clustering analysis support this proposed unit delineation. Our observations suggest that interglacial warming first uncovered basal diamicton. It is covered by remnants of basal ice or firn (unit 1, unit 2) after which ice-free conditions established a depositional environment that began with colluvial slumping (unit 3) and transitioned to a small fluvial system of increasing energy (units 4-5).

Together, analyses on the Camp Century subglacial sediment indicate a diverse stratigraphy preserved below the ice and capture episodes of glaciated and deglaciated conditions in northwestern Greenland. Our physical, geochemical, and mineralogic analyses reveal a history of deposition, weathering, and sediment transport preserved under the ice and show the promise of subglacial materials to increase our knowledge of past ice sheet behavior over time.

ACKNOWLEDGEMENTS

A special acknowledgement to my friends and community at UVM. The CosmoLab folks

have been such a wonderful lab group to be a part of. Lee, Halley, Bella, Peyton, Juliana,

and Jason, you all have made my time here so special. This acknowledgement would be

incomplete without mentioning all the wonderful people in the grad office. Bren, Sonya,

Emma, Niara, and Jillyan, you are all such strong intelligent women. I am so grateful to

call you all friends! I absolutely would not have survived the winters in Vermont without

such a wonderful community of people I am so impressed by.

Finally, thank you to my family. To my parents Sue and Michael for supporting me so

much while I have been so far from home. And thank you, Jack. You are my favorite part

of the day, a respite from the stress of grad school, and a selfless supporter. I am so

grateful Vermont brought me to you.

TABLE OF CONTENTS

LIST OF TABLES

---

[1] Sample names notation described in (Bierman et al., 2024)

[2] SEM (low magnification) denotes samples used for the image analysis performed on all available particles at a lower resolution for morphology analysis. Whereas SEM (high magnification), indicates the samples analyzed for use in the PCA and K-mean clustering.

LIST OF FIGURES

CHAPTER 1: INTRODUCTION

The Arctic is warming at a faster rate than any other region on Earth (Manabe & Stouffer, 1980). Arctic amplification, characterized by increased temperature in high latitude regions, ranges from 1.5 to 4 times global mean temperatures (Rantanen et al., 2022). Specific feedback loops, like the ice-albedo interaction, during which melting of the highly reflective ice leaves behind darker areas of ocean and land that absorb more incoming solar energy, drive the amplified warming (Manabe & Stouffer, 1980).

Greenland is losing ice mass at an increased rate due to this sustained elevated temperature (Smith et al., 2020). This is concerning because mass loss (melt) from Greenland's ice sheet alone could lead to more than 7 meters of sea-level rise (Box et al., 2022). If we continue with the current rate of carbon emissions, ice sheet mass loss and subsequent sea-level rise will threaten the viability of coastal cities and nations (Dutton et al., 2015), potentially affecting the 1.81 billion people exposed to high flood risk (Rentschler et al., 2022).

The key to understanding the future of Greenland melt lies in records of past ice-free events. The Pleistocene, the geologic epoch that occurred between 2.58 million to 11,700 years ago, is the most recent time in history when Earth experienced repeated glaciations and deglaciations. Referred as Marine Isotope Stages (MIS), these glacial and interglacial periods provide useful analogues for times when Earth's atmosphere was as warm or warmer than it is now (Lisiecki & Raymo, 2005). Scientists often look to MIS 5e (119 to 127 ka) and MIS 11 (374 to 424 ka) as analogues for the future of Greenland ice sheet (GrIS) melt and contribution to sea-level rise. This is because both had similar CO_2

concentrations to the pre-industrial era but had slightly higher global average temperatures (Kukla et al., 1997; Loutre & Berger, 2003).

During MIS 5e, the last interglacial, atmospheric CO_2 peaked at a concentration similar to preindustrial levels (Lüthi et al., 2008) and sea level at that time is estimated to have been 6-9 m above modern levels (Dutton et al., 2015). Though global temperature was about 2°C warmer than pre-industrial, studies show that the GrIS shrank minimally (Bender et al., 2010; Johnsen et al., 2001; Suwa et al., 2006a; Svensson et al., 2011; Willerslev, Cappellini, Boomsma, Nielsen, Hebsgaard, Brand, Hofreiter, Bunce, Poinar, Dahl-Jensen, Johnsen, Steffensen, Bennike, Schwenninger, Nathan, Armitage, De Hoog, et al., 2007; Yau et al., 2016).

MIS 11 was the longest and warmest interglacial during the Pleistocene. Global average temperature during this time is uncertain but most estimates suggest temperatures up to 2°C higher than pre-industrial levels (Dutton et al., 2015; Jouzel et al., 2007). Atmospheric CO_2 peaked at 286 ppm, again similar to preindustrial levels (Lüthi et al., 2008), and the sea level was 6 to 13 meters above modern levels due to GrIS, mountain glaciers, and Antarctic mass loss (Dutton et al., 2015). Pollen studies indicate the development of a boreal coniferous forest in southern Greenland which would require the ice to fully retreat from the region (Reyes et al., 2014; de Vernal & Hillaire-Marcel, 2008). Other studies focused on MIS 11 suggest southern GrIS collapse (Reyes et al., 2014b), northwestern GrIS retreat (Christ et al., 2023), but persistence of the ice sheet in the eastern highlands (Bierman et al., 2016). All scenarios, though, indicate a smaller GrIS extent and subsequent sea-level rise.

Two common methods used to infer the climate of the Pleistocene rely on ice cores and marine cores of ice rafted glacial debris. With ice cores, scientists often study ancient atmosphere trapped in bubbles in the ice, water stable isotopes, and volcanic tephra. Marine sediment cores utilize the presence of ice-rafted debris, which are materials transported by icebergs that deposit on the ocean floor when the ice melts (Bond et al., 1992; Grousset et al., 1993; Johnsen et al., 2001; Lisiecki & Raymo, 2005). Both necessitate the presence of ice in the past. When the ice was gone, we cannot use these methods as easily to understand paleoclimate. In this case, preserved sediment beneath the ice can reveal crucial information about ice-free events, their duration, and specific surface processes that occurred with in-situ physical evidence to expand our understanding of Greenland's paleoclimate that is not recorded in ice (Bierman et al., 2014; Christ et al., 2021, 2023).

Basal material drilled and recovered from below the GrIS has received less attention than the ice cores since the various drilling projects ended. Of the drilling projects Camp Century, NEEM, GRIP, GISP2, and Dye-3 retrieved either basal material or silty ice (Blard et al., 2023; Christ et al., 2021; Gow & Meese, 1996; Souchez et al., 1994, 1998; Willerslev, Cappellini, Boomsma, Nielsen, Hebsgaard, Brand, Hofreiter, Bunce, Poinar, Dahl-Jensen, Johnsen, Steffensen, Bennike, Schwenninger, Nathan, Armitage, De Hoog, et al., 2007). Of all of these, the Camp Century sub-glacial materials core is the most substantial, containing 3.44 meters of frozen sediment and ice (Hansen & Langway, 1966b). This sediment core is made up of several units, the deepest being older than 1.5 million years (Christ et al., 2021). Data show the top portion was last exposed to light about 416,000 years ago, which places it during MIS 11 (Christ et al., 2021, 2023). From this

core, we can gather information about past environmental processes and sea-level rise which can aid in our understanding of the more recent interglacials.

My thesis investigates physical, chemical, and mineralogic stratigraphy of the core sediments to uncover past environmental processes on Greenland during glacial and deglaciated times and supports other studies investigating this same core. Understanding the physical makeup of the Camp Century basal sediments improves our interpretation of the origins of the sediments. This thesis is integral to a joint effort to reconstruct the paleoclimate at the Camp Century drill site in Greenland 400,000 years ago and beyond. In addition to understanding the past climate, we will also be able to better understand past surface processes in a glaciated and deglaciated Greenland as well as post depositional processes.

In this thesis Chapter 1 serves as introductory information pertinent to the study. Chapter 2 is a manuscript prepared for submission to The Cryosphere that comprises the body of work I have done for my Master's degree. This is expected to be submitted for peer review in June 2024. Chapter 3 includes a reflection on my work on this project including what I would change if I had the chance to do this project over again.

CHAPTER 2: PHYSCIAL CHARACTERIZATION OF CAMP CENTURY

2.1 Introduction

Understanding past ice-free times allows us to predict the response of the Greenland Ice Sheet (GrIS) to current and future climate warming (Gemery & López-Quirós, 2024). This goal, deciphering Greenland's paleoclimate and ice sheet stability, has driven the ice core collection efforts since the 1950s (Bader, 1962). Deep ice coring in Greenland began in 1960 at Camp Century, a military camp in northwestern Greenland, ~200 km inland from the ice margin (Langway, 2008) (Fig. 1). The creation of this camp was one of numerous American responses to the perceived Russian threat in the arctic during the Cold War (Clark, 1965).
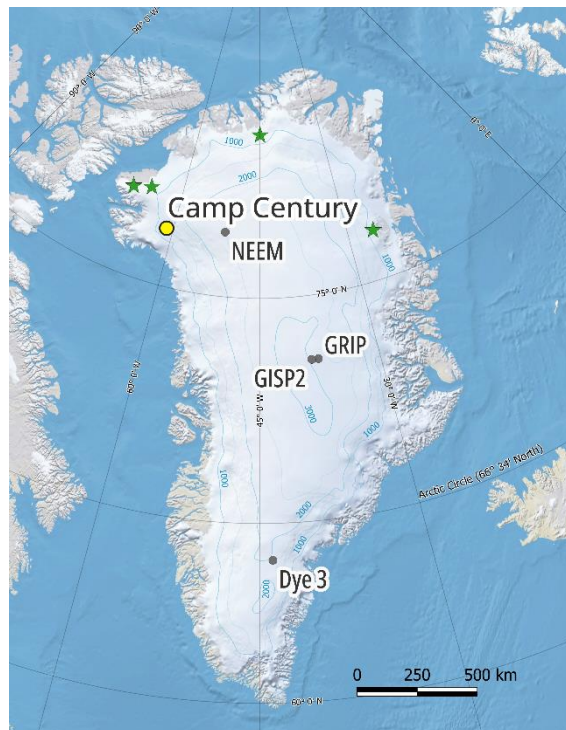
Figure 1. *Map of Greenland showing drilling locations where sub-glacial material has been received. Drilling locations for the ongoing GreenDrill project (Prudhoe Land, Hiawatha Margin, Victoria Fjord, and Dronning Louise from West to East) are marked by a green star.*

At Camp Century (77.2ºN, 61.1ºW), the U.S. Army drilled the first deep ice core that entirely penetrated an ice sheet. Additionally, they collected 3.44 m of sub-glacial material which would be the largest sub-glacial archive for the next six decades (Balter-Kennedy et al., 2023; Langway, 2008). The ice from this core was studied extensively (e.g., Hansen & Langway, 1966a; Johnsen et al., 1972; Langway & Hansen, 1970; W. Dansgaard et al., 1969) but the sub-glacial material was left relatively untouched save for a handful of studies (Fountain et al., 1981; Harwood, 1986; Whalley & Langway, 1980). The sub-glacial material did not move to the US Ice Core Repository with the rest of Camp Century core in the mid-1990s and was thought, by US researchers, to have been lost. It's rediscovery in 2019 in freezers of the Niels Bohr Institute at the University of Copenhagen sparked new interest in analyzing this unique archive (Bierman et al., 2024; Voosen, 2019).

The Camp Century sub-glacial core contains 3.44 meters of basal materials (Hansen & Langway, 1966b). It is made up of several units, the deepest made up of sediment last exposed to sunlight and cosmic radiation between 1.5-3.2 Myr (Bierman et al., 2024; Christ et al., 2021). Data show that the top of the core was exposed at the surface 416,000±38,000 years ago, which places its last exposure during Marine Isotope Stage (MIS) 11 (Christ et al., 2021, 2023). MIS 11 (374 to 424 ka) was both a long and warm interglacial with a peak atmospheric CO_2 concentration similar to pre-industrial levels (Dutton et al., 2015). This makes MIS 11 an important but imperfect analogue by which to study the effects of future warming (Dutton et al., 2015; Jouzel et al., 2007; Lisiecki & Raymo, 2005; Lüthi et al., 2008). The presence of plant and invertebrate

fossils in the Camp Century sub-glacial core mandates the site was not covered by ice during MIS 11 and indicates the maximum limit for ice extent at that time (Christ et al., 2021, 2023).

In this study, we used multiple physical, geochemical, and mineralogic techniques to characterize 26 of the 30 samples cut from the 3.44-meter Camp Century sub-glacial sediment core (Bierman et al., 2024). Our analyses refine the understanding of sub-glacial materials collected from below the GrIS at Camp Century in 1966. We employed a multi-scale technique to define sequence stratigraphy and analyze facies in order to infer what environments were present when this sediment and ice were deposited. At the macro-scale, we conducted a mineralogical survey using X-ray diffraction (XRD) to model quantitative relative mineral assemblages. At the meso-scale we utilized non-destructive micro-computed tomography (μCT) of the frozen sediment to make detailed stratigraphic observations at the tens of microns scale. We used scanning electron microscopy (SEM) and associated geochemical mapping to analyze grain coatings, textures, and shapes at the micron scale. Using non-destructive μCT in tandem with other methods (XRD, SEM) allowed us to maximize data output when working with a volumetrically limited archive. Characterizing this unique sub-glacial core provides the opportunity to expand our knowledge of Greenland's climatic history, interglacial surface processes, and sub-glacial processes.

2.2 Background

Sub-glacial material is a valuable source of both paleoclimate and glacial process information (Bierman et al., 2014; Schaefer et al., 2016). Sediment preserved beneath the

ice and in basal ice can reveal crucial information about ice-free events, their duration, and specific surface processes. Basal materials are particularly important because they contain in-situ physical evidence for past events that are not recorded in glacier ice (Bender et al., 2010; Bierman et al., 2014; Blard et al., 2023; Christ et al., 2021, 2023; Gow & Meese, 1996; Marschalek et al., 2024; Schaefer et al., 2016; Suwa et al., 2006b; Yau et al., 2016).

2.2.1 Basal Ice

Nearly every deep ice core from the GrIS (Camp Century, Dye 3, Greenland Ice Sheet Project - GISP2, Greenland Ice Core Project - GRIP, and North Eemian Project - NEEM) has retrieved meters of deformed ice containing bed material, referred to as silty ice or basal ice (e.g., Bender et al., 2010; Blard et al., 2023; Christ et al., 2021; Gow & Meese, 1996; Hansen & Langway, 1966a; Souchez et al., 1998; Suwa et al., 2006). The basal ice layer (BIL), located above the ice-bed interface, is predominantly influenced by processes operating at and near the bed – specifically deformation, regelation, and in some cases melting. This limits the interpretability of the climate record in the deepest ice, but the sediments entrained in the basal ice can reflect aspects of glacial and sub-glacial processes as well as paleoenvironmental conditions (Knight, 1997).

Initial analyses of debris in the Camp Century BIL confirmed, using SEM and XRD analysis, that the sediment originated from the frozen material below (Herron et al., 1979). In other cores, investigation of ancient biomolecules in Dye 3 and GRIP silty ice found evidence that a boreal forest once existed at Dye 3 which necessitates extensive ice sheet retreat from southern Greenland (65.2°N), but such retreat did not appear to reach

as far north as GRIP (72.5°N) (Willerslev et al., 2007). Stable water isotope composition of the BIL in the GRIP core, corroborated by a comparative study between the debris found there and at GISP2 (72.5°N), indicates that the BIL originated as ground ice before incorporation into the larger growing ice sheet and has since deformed (Gow et al., 1997; Gow & Meese, 1996; Souchez et al., 1994, 1995; Tison et al., 1994). A multiproxy analytical approach applied to sediment in the BIL from the NEEM core (77.5°N) (Blard et al., 2023) found evidence of a sequence of glacial retreat and advance possibly similar to that which has been identified in the Camp Century sub-glacial material (Christ et al., 2021, 2023).

2.2.2 Sub-glacial Material

In Greenland, coring activities at Camp Century, GISP2, and GreenDrill retrieved sub-glacial material from beneath the ice-bed interface (Balter-Kennedy et al., 2023; Christ et al., 2021; Gow & Meese, 1996; Souchez et al., 1994, 1998). At GISP2, drillers extracted 48 cm of till (mostly boulders, only 8-10 cm fine grain material) and 1.07 m of underlying rock (Gow et al., 1997). Cosmogenic isotopic analysis of that rock and till indicates that the land surface at GISP2 was deglaciated for extended periods of time during at least one and possibly many Pleistocene interglacials (Bierman et al., 2023; Schaefer et al., 2016). Grain texture analysis of Camp Century sediments (Whalley & Langway, 1980) revealed two populations of grains mixed sub-glacially: angular grains, attributed to glacial crushing, and rounded grains, attributed to aeolian transport. Whalley & Langway (1980) infer that the aeolian fraction must have been produced before the ice advanced, mandating prior ice-free conditions. A petrographic investigation of 17 clasts

in the Camp Century sub-glacial core revealed that they were compositionally similar to those cropping out at the ice sheet margin (Fountain et al., 1981). Extraction of fresh-water diatoms from the bottom of the Camp Century BIL and the upper portion of the sub-glacial core indicates that the ice retreated far enough to expose the Camp Century drill site at least once during the Pleistocene (Harwood, 1986). Cosmogenic and luminescence dating of the upper and lowermost sub-glacial samples indicate that the 3.44 m of material records at least two glaciations separated by ice-free conditions during MIS11 (Christ et al., 2021, 2023). The currently active northern Greenland drilling project, GreenDrill, has successfully retrieved 3 m of silt to cobble-sized sediment in basal ice atop 4.5 m of gneiss bedrock with the intent to use cosmogenic exposure and burial dating to further constrain past ice-free events in Greenland (Balter-Kennedy et al., 2023; Briner et al., 2022).

2.2.3 Computed Tomography

Computed tomography (CT), a technology widely used in the medical field, is also a powerful tool for examining sediment cores non-destructively (Renter, 1989). CT scans produce greyscale images based on the intensity of the attenuated X-ray beam (i.e. CT number) and are reconstructed to produce 3-dimensional (3D) models of the scanned object (Razi et al., 2014). CT scans have been leveraged to do quantitative facies characterization by comparing density plots that suggest environmental changes (Emmanouilidis et al., 2020; Lee et al., 2021). Used in studying marine sediment cores, CT scans aided in calculating bulk density and its spatial variation vertically and laterally

(Orsi et al., 1994). CT scans also provide detailed visualizations of sediment structures, grain distribution, and material densities (Mena et al., 2015).

CT scanning technologies are effective in studying frozen permafrost cores. Some studies have characterized the sediment properties, cryostructures, and ground ice content of permafrost but did not find CT successful as a proxy for identifying ground ice origin (Calmels & Allard, 2008; Lapalme et al., 2017). Micro CT (μCT), a refinement of this technology, provides micron-scale resolution (typically between 1-150μm voxels) for more detailed studies and has been used to make pore-scale observations (Lei et al., 2018, 2022). Three-dimensional microstructure analysis in permafrost allows for quantification of physical properties, including the spatial density of ice inclusions, which can be useful in estimates of thermal conductivity (Nitzbon et al., 2022). The same authors suggest that microstructure analysis from μCT scans, in combination with other measurements, allows for reliable inference of depositional processes (Nitzbon et al., 2022).

2.2.4 Microscale Grain Characteristics

Grain characteristics have been used routinely to inform sedimentological studies (Naqshband & McElroy, 2016). Grain size distribution is understood to be a possible indicator of transport energy, as higher energy fluids can transport larger/heavier grains (Gresina et al., 2023; Hjulström, 1935; Malusà et al., 2016). Specific grain morphology, including roundness and circularity, are related to transport energy, transport distance, mode of transport, and conditions at the site of deposition (Krumbein, 1941). Recently, studies of grain morphology have used automated image analysis (Gresina et al., 2023; Szmańda & Witkowski, 2021; Tafesse et al., 2013) to infer

11

transport mechanisms. For example, properties of particle shape, investigated using this method, correlate circularity and roundness with transport distance and energy, respectively (Gresina et al., 2023). Image analysis of sediment grains from coastal dunes shows that roundness and patterns in size and shape indicate various and specific modes of transport in aeolian sediments (van Hateren et al., 2020). Quartz morphology, including roundness assessments and microstructures, has revealed evidence of past storm frequency and has been used to reconstruct sediment provenance and transport in NW Poland during the Last Glacial Maximum (Kalińska-Nartiša et al., 2018; Woronko et al., 2015). Grain size analyses of loess deposits identify episodes of rapid climate change, which mimic rapid climate fluctuations during the last glacial period (Dansgaard-Oeschger events) that have been identified in ice cores (Vandenberghe & Nugteren, 2001).

Grain coating abundance and distribution can also provide information of original transport mechanism and post-depositional processes. Coatings on grain surfaces indicate post-depositional weathering processes in both temperate and in Arctic regions where geochemical processes play an important role in in situ weathering (Dixon et al., 2002). Notably, the absence of grain coatings signals an active transport environment (Musselman & Tarbox, 2013). Glacial flour is also common in these deposits and is characterized by agglomerates of clay to silt-sized angular particles typically dominated by feldspars (Pesch et al., 2022).

2.2.5 Cryostratigraphy

Cryostratigraphy describes the shape, amount, and distribution of ice and sediment in frozen ground (Murton & French, 1994). Cryofacies are defined by distinct patterns of ice lenses, volumetric ice content, and layering of ice and sediment. Cryostratigraphy helps infer permafrost formation mechanisms as either *epigenetic*, permafrost that forms after sediment deposition, or *syngenetic*, permafrost that forms as material is being deposited (French & Shur, 2010). Ground ice includes pore ice and segregated ice but typically excludes buried ice (French & Shur, 2010; Murton & French, 1994). Pore ice operates as cement, holding the sediment together. Segregated ice forms as ice accumulates along the freezing plane, the boundary between conditions supporting liquid water and ice, and can be millimeters to tens of meters thick (French & Shur, 2010). Organized lenticular and layered cryostructures are common in syngeneic permafrost and tend to be short, thin, and highly abundant (French & Shur, 2010; Murton & French, 1994). Epigenetic permafrost is typically characterized by reticulate cryostructures that reflect shrinking as sediment freezes, a phenomenon most common in fine-grained sediments (French & Shur, 2010). Thaw unconformities occur and are identified by the presence of epigenetic structures bordering diagnostic syngenetic features (French & Shur, 2010). In modern cryostratigraphy, CT scan images have been used successfully to identify cryostructures in permafrost from the McMurdo Dry Valleys of Antarctica (Lapalme et al., 2017).

2.3 Methods

The Camp Century sediments are well preserved despite their spending at least hundreds of thousands of years buried under almost a mile of ice. Because of the high level of preservation, we employed standard geologic practices to study the stratigraphy and mineralogy of the sub-glacial materials. We used frozen samples for µCT, and after thawing at 4°C, we used bulk sediment for XRD and SEM analysis on a total of 26 samples from the archive. For the µCT analysis, we utilized two subsamples per core section (subsequently referred to as (a) and (b)), for a total of 49 subsample scans. Bierman et al. (2024) describe the core cutting and allocation procedure in detail.

2.3.1 Micro-Computed Tomography

We created a digital archive of the (a) and (b) sub-samples, 49 in total, by collecting a series of µCT scans. We scanned sub-samples (a) and (b) from each core section using a Bruker SkyScan1173 µCT scanner fit for use in a cold room at -10°C at the Cold Regions Research and Engineering Laboratory (CRREL) in Hanover, NH. Each of the ~10 cm-tall samples were scanned in two overlapping 7.9 cm-tall sections at a resolution of 71 µm/voxel to capture the entire length of the sample. We completed reconstructions for each scan using the Bruker NRecon software. This resulted in 84 partial sample scans, 7 full sample scans, and 8 zoomed scans. Two scans resulted in failed reconstructions due to difficulty with the scanning procedure. The raw data is archived with the Arctic Data Center.

Scanned sections of each sub-sample of the core were merged using a globally optimal stitching algorithm ("*Stitching*" Fiji plugin) (Preibisch et al., 2009; Schindelin et

al., 2012). This was generally unsuccessful because, to avoid melting, the overlapping scans were not registered 3-dimensionally during the scanning process. While these stitched scans are useful for visualization, there are artifacts in the overlapping sections of some samples that prevent quantitative analysis of the stitched models.

Qualitative assessment and 3D visualization of the partial scans, using Bruker's CTVox software, allowed us to investigate contacts, layering, sorting, lineations, and permafrost features of each sample. The 3D nature of the CT scans allows us to look at internal structures by slicing into the models laterally. We also were able to filter the CTVox interface to only display the denser suspended particles to look for other structures such as layering and particle alignment. Angularity of larger grains were also assessed visually defining angular grains as having sharp edges and rounded grains as having smooth, curved sides including intermediate assessments between these categories (Janoo, 1998).

2.3.2 X-ray Diffraction

We analyzed the crystalline composition of selected core samples by XRD using a Rigaku MiniFlex II, equipped with a Cu X-ray tube. Following qualitative diffractogram analysis, we quantified the diffractograms using the Rietveld Full Pattern Profile Fit algorithm included in the PDXL-2 software (PDXL, Rigaku Corp). Our analysis used a representative group of 15 samples from various sections of the sub-glacial core (Table 1). We used approximately 0.2 g of bulk sediment from each sample and ground it manually with a mortar and pestle. The ground sediment was mounted on a zero-background plate in random orientation mounts and analyzed in 2theta-theta geometry

15

between 3 and 70 °2θ with a dwell time of 1 degree/min and 0.02 °2θ resolution for a

total run time of 67-minutes. We characterized the mineralogy using databases from the

International Center for Diffraction Data 2.0 and Crystallography Open Database for

peak matching. Subsequently, we performed quantitative analysis of the X-ray

diffractograms using a semi-automatic Rietveld approach (Rietveld, 1969). To refine our

results, we varied the values for scale factor, cell parameters (within 0.2Å), shape

parameters, and for selected minerals (clays and amphiboles), the March–Dollase

preferred orientation parameter, similarly to the methodology described in Mackowiak

and Perdrial (2023).

2.3.3 Scanning Electron Microscopy Imaging and Energy Dispersive X-ray Micro-mapping

For SEM imaging, we embedded thawed bulk sediments taken from subsamples

(a) and (b) (Table 1) in epoxy resin (EPO-TEK 301). After curing for at least 24 hours,

we micro-polished the resulting epoxy puck using a decreasing grit size to 0.05 μm. The

mounts were carbon sputter-coated prior to analysis in backscattered electron (BSE)

mode using a TESCAN VEGA3 scanning electron microscope coupled with an Oxford

Instruments Aztec Elemental Mapping Energy Dispersive X-ray Spectrometer (EDS) in

the Geology Department at Middlebury College. We acquired BSE images and EDS

maps at 20 keV for a minimum of 20 frames totaling 10-minute elapsed time for each

multi-elemental map. Then, we generated multi and tri-color maps using the Gatan digital

micrograph 3.1 software. We imaged 15 samples with the SEM and analyzed 2 sites on

each mount (except sample 1059-6 which was imaged only at one site) resulting in 29 individual images.

Grain coating evaluation was conducted over all 29 images. To do so, we used the EDS maps to evaluate each grain and placed it, based on grain coating abundance, into the following five unique categories: grains dominated by coating (>50% coverage), grains with moderate coating (<50% and >25% coverage), grains with little to no coating (<25% coating), grains with coating only in cracks, and fine particle aggregates. Observations from two sites of the same samples were merged so that there is one summed evaluation per sample. Counts were converted to percentages so as to normalize data between samples. We created the category "High Abundance" which comprises the dominated and moderately covered by coating categories to communicate abundance vs. depth more succinctly.

We acquired another set of SEM images in BSE at a lower resolution for grain size and shape analysis of all mineral compositions. Images at the lower resolution were collected for 9 samples throughout the core. The 9 samples were mounted in epoxy and coated with 10 nm carbon to make them conductive. Backscattered electron contrast (BSE) images were generated at the ZEISS Sigma 300 VP equipped with a field emission gun, using the ZEISS Mineralogic™ software platform. A mosaic of BSE frames of a representative part of the sample was taken. Further details on the software and applied method can be found in Keulen et al. (2020). Analyses were performed with acceleration voltages of 15kV, a 120 μm^2 aperture.

Table 1: Summary of samples[3] and physical, geochemical, and mineralogic analyses performed.[4]

Core Tube	Sample	Depth (cm)	XRD	SEM (low magnification)	SEM (high magnification)	µCT scans
1059	1059-5	10-20	Analyzed	Not run	Analyzed	Scanned
	1059-6	20-29.5	Analyzed	Analyzed	Analyzed	Scanned
	1059-7	29.5-34	Analyzed	Not run	Analyzed	Scanned
1060	1060-A1	34-44.5	Not run	Analyzed	Not run	Scanned
	1060-A2	44.5-55.5	Analyzed	Not run	Analyzed	Scanned
	1060-B	55.5-78.5	Analyzed	Analyzed	Analyzed	Not scanned
	1060-C1	78.5-88.5	Analyzed	Analyzed	Analyzed	Scanned
	1060-C2	88.5-98.5	Analyzed	Not run	Analyzed	Scanned
	1060-C3	98.5-108.5	Not run	Analyzed	Not run	Scanned
	1060-C4	108.5-118	Not run	Not run	Analyzed	Scanned
	1060-C5	118-129	Not run	Not run	Not run	Scanned
1061	1061-A	129-137	Analyzed	Not run	Not run	Scanned
	1061-B	137-159	Analyzed	Not run	Analyzed	Not scanned
	1061-C	159-171	Not run	Analyzed	Not run	Scanned
	1061-D1	171-181	Not run	Not run	Not run	Scanned
	1061-D2	181-191	Analyzed	Not run	Not run	Scanned
	1061-D3	191-201	Not run	Analyzed	Analyzed	Scanned
	1061-D4	201-215	Missing	Missing	Missing	Missing
	1061-D5	215-223	Analyzed	Not run	Analyzed	Scanned
1062	1062-1	223-231	Analyzed	Not run	Analyzed	Scanned
	1062-2	231-238	Not run	Not run	Not run	Scanned
	1062-3	238-250	Analyzed	Not run	Analyzed	Scanned
	1062-4	250-263	Not run	Analyzed	Not run	Scanned
1063	1063-1	263-273	Not run	Not run	Not run	Scanned
	1063-2	273-283	Analyzed	Not run	Analyzed	Scanned
	1063-3	283-294.5	Missing	Missing	Missing	Missing
	1063-4	294.5-305.5	Not run	Not run	Not run	Scanned
	1063-5	305.5-317	Not run	Not run	Not run	Scanned
	1063-6	317-327	Analyzed	Analyzed	Analyzed	Scanned

---

[3] Sample names notation described in (Bierman et al., 2024)

[4] SEM (low magnification) denotes samples used for the image analysis performed on all available particles at a lower resolution for morphology analysis. Whereas SEM (high magnification), indicates the samples analyzed for use in the PCA and K-mean clustering.

2.3.4 Image Analysis

We postprocessed the chemical maps to determine grain size and grain shape parameters of quartz grains only (Table 1) using Fiji (Schindelin et al., 2012; Vandel et al., 2020). To isolate quartz grains, we used multielement color maps created with Gatan's Digital Micrograph (from the EDS data) and we performed a color threshold to select the Si-O only phases (quartz). We then performed particle analysis on the Fiji platform. We measured three grain size/shape parameters (area, roundness, and circularity) and stored the average and standard deviation for each parameter. Fiji calculates circularity as $4\pi(Area/Perimeter^2)$, which returns values between 0-1, where a value of 1.0 indicates a perfect circle. Roundness is calculated as $4*Area*(\pi*major\ axis^2)$, which returns values between 0-1, where larger values indicate increasing roundness.

We performed another image analysis on the set of SEM images acquired at a low magnification, allowing for a larger dataset. For this analysis, we included all grain compositions. The parameters grain size, circularity and roundness were measured using particle analysis in Fiji and a Tukey-Kramer HSD pair-wise comparison was performed on the means for each sample in JMP Pro 15.0.0 (*JMP*, 2024). In all cases the significance level (α) was set at 1%. To represent significance between classes, we report differences using connecting letters for simplicity where levels not connected by the same letter are significantly different.

2.3.5 PCA Analysis and K-means Clustering

Methods for reducing the dimensionality of a dataset, including principal component analysis (PCA) and K-means clustering, can be useful when interpreting

physical grain characteristics and geochemical aspects (Jansson et al., 2022). To assess

our unit assignments, we performed a PCA analysis and K-means clustering on data from

our image analysis of quartz grains. The size and shape parameters (including standard

deviations) from the image analysis, combined with percent ice composition, percent

fine-grained fraction composition, percent quartz composition, depth, and an ordinal

evaluation of grain coatings varying from 0-2 (no coating, minimal coatings, and

extensive coatings) were used as input variables in a K-means clustering method. The

data set includes the 11 variables mentioned above, measured over a total of 29

observations from the 15 samples. The cluster centers were calculated using a "nearest

centroid sorting" approach (Anderberg, 1973; *JMP*, 2024). We performed a PCA to

understand the driving factors in clustering patterns. We then performed a K-means

clustering in JMP Pro 15 to assess the optimal number of clusters according to the cubic

clustering criterion. Z-score values of all variables in each cluster were calculated in R (R

Core Team, 2022).

2.4 Results

Our multiscale analysis supports and refines the proposed unit delineations in

Bierman et al. (2024). Size distribution shows at least 16% abundance of very fine sand

and silt-sized grains in all units (in some units the abundance of fines is over 90%) and

more variability in size in the lower portion of the core. Grain coatings increase in

abundance with depth and are largely absent in the upper two units (4 and 5). Grain shape

analysis (roundness and circularity) does not vary systematically within or between units.

PCA and a K-means analysis quantitatively corroborate our understandings of these systems.

2.4.1 Micro-Computed Tomography
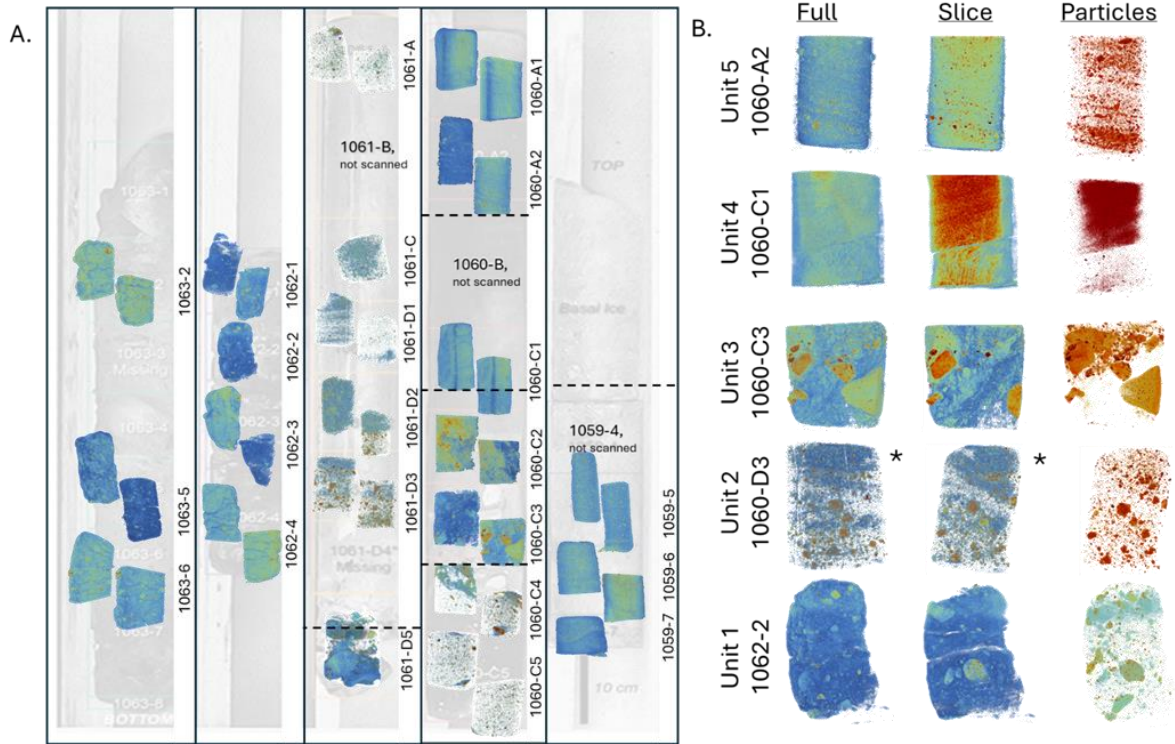
Figure 2. *(A) CT scans layered over historical image of original core (Fountain et al., 1981). Scans were done in overlapping sections, each individual scan is ~7cm tall. Samples not scanned are noted and missing samples from the archive are shown as gaps. Dashed horizontal lines denote unit delineations. (B) Selected representative samples per unit. Samples 1060-A2, 1060-C1, 1060-C3, and 1062-2 are shown with three views, a full view, an internal slice, and a filtered view of just the dense suspended particles. The first two examples of 1060-D3, marked by an asterisk, show different angles of the sample to show the vertical clear ice inclusions and strong banding. Note that the orientation between samples is not known as no note of the core orientation exists in the archive.*

MicroCT scans show that the lowermost 7 samples define a homogeneous unit

(Unit 1; 223-327 cm depth below the ice-sediment interface) – a diamicton displaying a

variety of cryostructures (Fig. 2a). These 7 samples are characterized by variably sized

21

clasts (ranging from angular to sub-rounded and spherical to elongated) in a muddy matrix with no bedding. Throughout the unit, sub-horizontal ice lenses cut through the sediment in a braided lenticular pattern (see example in 1062-2, Fig. 2b). Although no clear difference exists between the sections, the topmost sample (1062-1) appears to contain more cryostructures.

The CT scan of sample 1061-D5 (215-223 cm) captures a transition in the type of deposition. The upper portion of the sample has a high ice content compared to the lower portion of the sample which is sediment-rich like the rest of Unit 1. The transition is not discrete as it consists of 2 ice-rich layers separating the dense fine-grained matrix material of Unit 1.

The next 6 samples (1061-D3 to 1060-C4) comprise Unit 2 (108.5-215 cm). They are characterized by high ice content with sediment interspersed throughout. The μCT scans show that sediment is generally fine-grained with few clasts and bedded at approximately a 45° angle from horizontal. The tilted bedding is more apparent in some samples (1060-D3, 1061-D1, and 1060-C4). Vertical fractures filled with clear ice create intersecting planes in the sediment-laden ice.

MicroCT scans of samples in Unit 3 (88.5-108.5 cm) show deformed bedding, normal grading, and some reticulate cryostructures. The samples in this unit are 1060-C3, 1060-C2, and the lower portion of 1060-C1 where there is an unconformable contact (at an angle of 11°) with the upper sediments, distinguishable by μCT scans (this contact is more apparent in subsample (b) whereas in subsample (a) the contact is nearly indistinguishable) (Fig. 2b). In samples 1060-C2 and below the contact in 1060-C1, there

is deformed fine-grained bedding with high ice content (49%) (Bierman et al., 2024).

Directly below the contact bedding curves from sub-horizontal, downward to nearly 90°

which continues into 1060-C2. In 1060-C3 there is no bedding visible, instead the sample

is comprised of pebble-sized clasts in a silt-sized matrix with lower ice content (23%)

(Bierman et al., 2024). Clasts range from sub-angular to sub-rounded. Cryostructures in

the silty matrix form a reticulate pattern in sample 1060-C3.

The 2 units above Unit 3 are similar in structure, with both containing well-sorted

bedded sand. Unit 4 (55.5-88.5 cm) includes sample 1060-C1 (the portion above the

contact) and 1060-B (not scanned). These sediments are bedded, well sorted, fine-grained

sand. Bedding in these samples are distinct, parallel, and sub-horizontal with a ~15° dip.

The well-sorted fine-grained nature of the deposit defines this unit.

Samples 1060-A2 to 1059-5 define Unit 5 (0-55.5 cm). These samples coarsen

upward into gravelly sand from the fine-grained sands of Unit 4. Bedding is well defined

in the lower samples in this unit (notably 1060-A2) and becomes harder to distinguish in

the top-most sample scanned (1059-5). The layers also dip at 15°. There are some small

pebble-sized clasts, which range from sub-rounded to sub-angular, that form individual

beds. Well-sorted sand-sized grains that coarsen upward with well-formed bedding define

the upper most portion of the core and the top of unit 5 (Fig. 2).

23

2.4.2 X-ray Diffraction
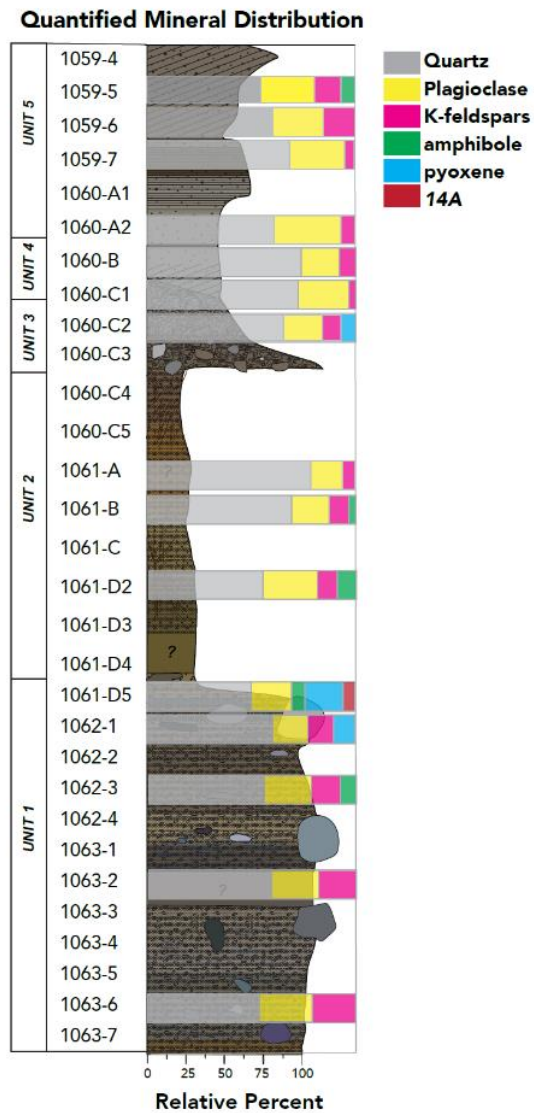
Figure 3. *Relative mineral assemblage of 15 samples shown with corresponding color bars. Relative percent was calculated using the Rietveld algorithm (Rietveld, 1969). Stratigraphic column adapted from (Bierman et al., 2024).*

XRD analysis indicates very little change in relative mineral abundance between units (Fig. 3). Throughout the core, the mineralogy is dominated by quartz with lesser amounts of plagioclase and potassium feldspar. The average quartz relative abundance

24

was 63.6%±3.9% with a minimum of 49.6% ± 0.7% (1061-D5, Unit 2) and a maximum of 80.6% ± 1.1% (1061-A, Unit 2). We found plagioclase in all units with an average of 22.4% ± 3.5%, with a minimum of 14.8% ± 1.1% (1061-A, Unit 2), and a maximum relative percent of 31.8% ± 1.3% (1060-A2, Unit 5). Potassium feldspar was detected in all samples except 1061-D5 (Unit 1), the average 10.5% ± 3.0% with a minimum of 3.1% ± 0.2% (1060-C1, Unit 3/4), and a maximum of 19.4% ± 0.8% (1063-6, Unit 1). Amphibole was found in low concentration in five samples: 1059-5 (0.4% ± 0.2%, Unit 5), 1061-B (2.3% ± 0.6%, Unit 2), 1061-D2 (7.0% ± 0.8%, Unit 2), 1061-D5 (5.6%±0.5%, Unit 1), and 1062-3 (6.1% ± 0.5%, Unit 1). Pyroxene was found in three samples: 1060-C2 (5.7% ± 0.5%, Unit 3), 1061-D5 (19.6% ± 0.7%, Unit 1), and 1062-1 (9.5% ± 1.6%, Unit 1). A 14Å "clay", most likely clinoclore, was detected in only 1061-D5 (4.9% ± 0.4%, Unit 1). The relative amount of quartz appears to steadily decrease from the bottom to the top of unit 5 whereas the relative amount of quartz increases from the bottom to the top of unit 2. For all other units, the relative proportions of quartz compared to other minerals remains similar.

2.4.3 Scanning Electron Microscopy Imaging and Energy Dispersive X-ray Micro-mapping

Small particles <2500 μm^2 (60 μm diameter calculated from the circular equivalent) are present in all samples, though the range of grain sizes differs per sample (Fig. 4a). Samples 1060-B and 1061-C contain 99.3% to 90.3% of particles with an area less than 2500 μm^2, respectively. Samples 1059-6, 1060-C3, 1061-D3, and 1063-6 have on average 58% ± 6.4% fines (area <2500 μm^2) and 1060-A1, 1060-C1, and 1062-4 have

an average of 19.5% ± 2.3% fines. Samples 1059-6, 1060-A1, and 1062-4 show a much

wider distribution of grain sizes (Fig. 4a). Pair-wise statistical analyses of grain size

distribution identify sample group 1059-6, 1060-A1 and 1061-D3, sample group 1060-B,

1061-C and 1063-6, and sample 1062-4 as statistically different from each other by

particle size.
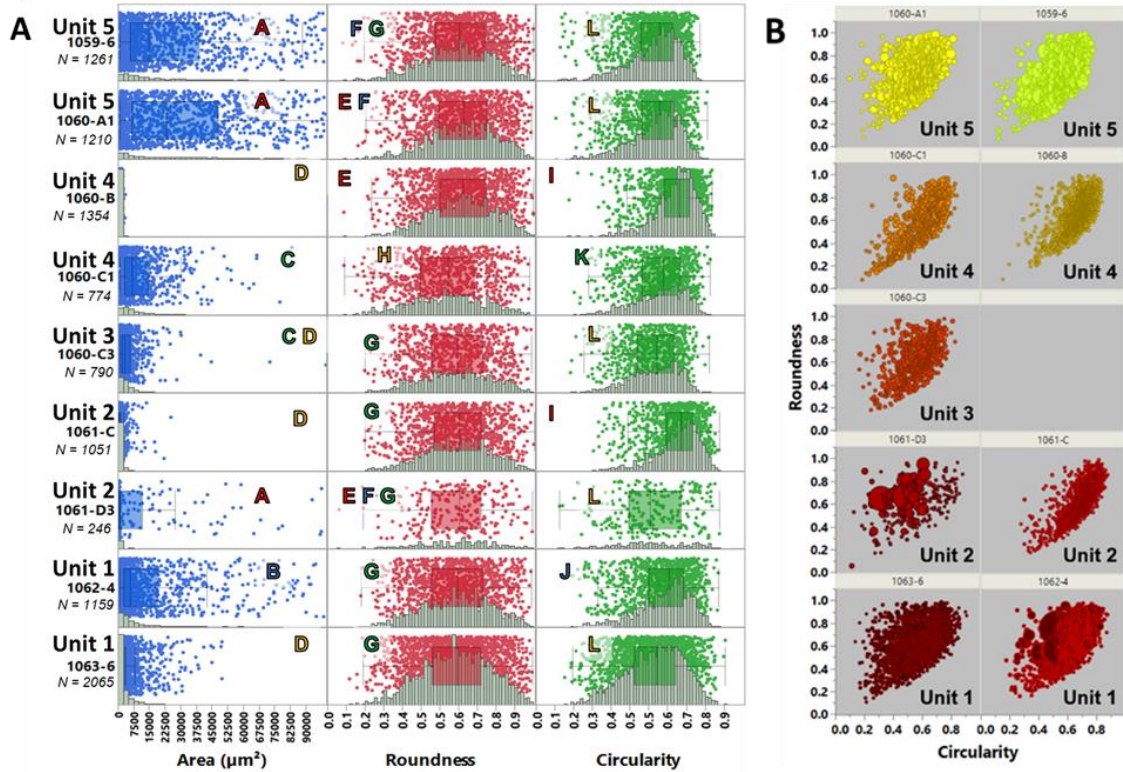
Figure 4. *Grain size and shape parameters extracted from low magnification SEM backscattered images of selected core samples. (A) Distribution of grain size, roundness, and circularity for individual samples, N represents number of particles examined. For simplification, the maximum area displayed is limited to 100,000 um². Roundness and circularity parameters were defined in section 2.3. The colored letters refer to the pairwise significance of means with similar letters indicating lack of significant differences. (B) Relationship between particle size, circularity, and roundness for selected individual samples. The size of the points represents the relative area of individual grains and points are colored according to sample names.*

The roundness parameter is consistently centered around the mean value of 0.62 ± 0.01 with a maximum value of 0.65 ± 0.005 (1060-B) and minimum of 0.58 ± 0.006 (1060-C1), indicative of moderate roundness. While all distributions of roundness are symmetric and unimodal, a Tukey-Kramer mean comparison tests shows that the data in sample 1060-C1 is significantly different from all other samples and that sample 1060-B is also significantly different from 6 of the 9 samples (Fig. 4).

Circularity values are consistently left skewed, towards higher circularity values, and all fail the Anderson-Darling test for normality. A Tukey-Kramer test splits the data into four groups with no overlap: (I) 1060-B and 1061-C, (J) 1062-4, (K) 1060-C1, and (L) 1059-6, 1060-A1, 1060-C3, 1061-D3, and 1063-6. These groups are very similar to the size distribution groups with the sole exception of sample 1060-C3. Comparing size, roundness, and circularity, larger grains tend to have a lower circularity and higher roundness (based on a significant negative and positive Pearson coefficient, respectively) (Fig. 4b).

EDS mapping analysis of SEM images reveals strong patterns with grain coatings and depth. Grain coatings and fine particle aggregates are most abundant in Unit 1 and are present in all Unit 1 samples (Fig. 5a, b). Unit 2 has a mix of fine particle aggregates, grain coatings, and clay aggregates, but not all grains have coatings and others are partially coated (Fig. 5a). Unit 3 has clay aggregates and grains that are partially coated (Fig. 5a). Units 4 and 5 have fewer grain coatings than the other units.

Elemental mapping using principal constituents Si, Fe, and Al allows us to identify quartz (high Si), feldspar and clay (high Al), and pyroxene and amphibole (high Fe) (Fig.

5a). Quartz and feldspar, including plagioclase, largely dominate all samples. A positive

correlation between the "high abundance" grain coating category (grains with more than

25% of grain coating around their perimeter) and core depth have a correlation

coefficient of 0.7 (Fig. 5b). Tukey-Kramer comparison by "high abundance" and unit

reveals that Unit 1 is different from all other units and that Unit 3 has similarities with

Unit 1 and all other units.
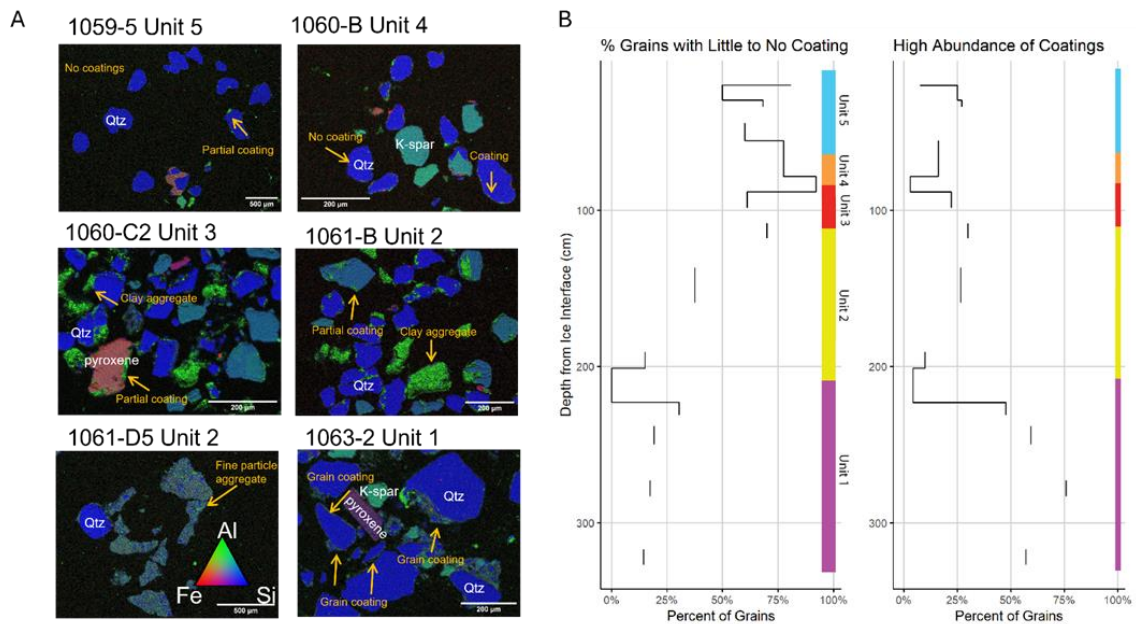
Figure 5. *(A) Scanning electron microscopy images showing mineral type and observed coatings. Blue color indicates high silicon content (quartz), green is associated with aluminum (clays and feldspars), and red is associated with iron. (B) Abundance of grain coatings down core showing percentage of grains with little to no coating and percent of coating with a high abundance of grain coatings (dominated and moderate categories combined). Colored bar shows unit assignments with depth.*

2.4.4 PCA and K-means Clustering

K-means clustering analysis, according to the cubic clustering criterion, indicates

optimal clustering occurs with 5 clusters (Figs. 6a, b). There are similarities with this

clustering and our unit assignments, most notably Unit 1 clusters together exclusively.

There is mixing between Units 3, 4, and 5 between Cluster B and Cluster C. Unit 2 has

samples within 3 different Clusters A, B, and D (Fig. 6b).
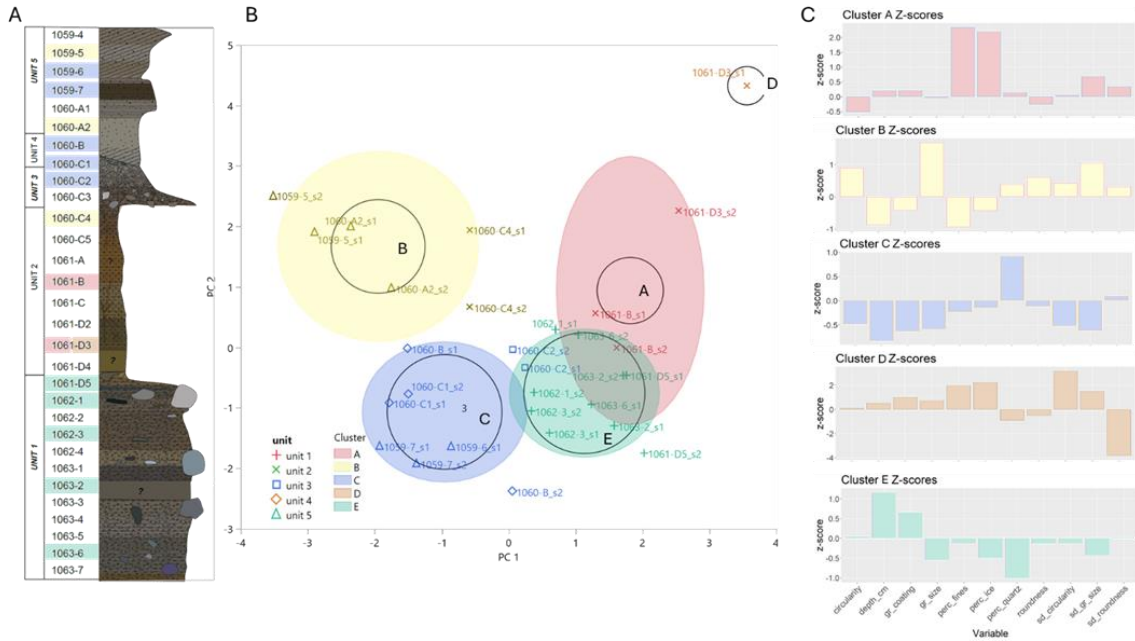
Figure 6. *(A) Stratigraphic column with samples highlighted according to the K-means clustering (B) Kmeans clustering analysis on multiscale physical, mineralogical and geochemical data. The data are plotted on a PCA, using principle component (PC) 1 and 2, and are categorized into 5 clusters. Individual clusters are color-coded and assigned a letter. Unit assignments are indicated by shape. (C) Z-scores of each cluster are shown which indicate how many standard deviations (y-axis) the mean of each variable in the cluster differs from the observed mean across all data. Z-score graphs all have the same x-axis variables in the same order as shown in the Cluster E graph.*

Significant variables associated with PC1 include depth, percent quartz, grain

coating, and percent fines. This principal component can be summarized as relating to

transport processes, as percent fines and percent quartz often reflect sorting that occurs

during transport and grain coatings are stripped during transport processes. Significant

variables associated with PC2 are grain size, standard deviation of grain size, standard

deviation of circularity, and circularity to a lesser extent. This component represents

aspects of grain morphology. According to PC1, transport process, there is a larger

29

separation between Clusters A and B than there is between E and C (Fig. 6b). Along PC2, clusters A and B are separated from Cluster C and E. Cluster D contains one sample belonging to Unit 2 (1061-D3) and it is positioned at extreme ends of both principal components indicating there is a strong difference between this sample and the rest of the data. The other observation associated with sample 1061-D3 (as two images were analyzed for this sample) is assigned to Cluster A. This observation is also positioned at high ends of both axes, as is the same for Cluster D.

Z-scores can be indications of the driving factors for clustering behavior and provide insight into why there may be disagreements between our unit assignments and the clusters (Fig. 6b, c). Z-scores for Cluster A, made up of Unit 2 samples, show the most significant factors are percent fines and percent ice with positive Z-scores of 2.3 and 2.2 respectively (indicating values for these variables are larger than the population mean in this cluster, comparatively) (Fig. 6c). This means Cluster A samples (Unit 2) have more fine-grained particles and more ice on average. Cluster B samples (mainly Unit 5) can be described as having larger grain size with slightly more size variation and slightly higher values of circularity on average (grain size Z-score=1.7, sd grain size Z-score=1.1, and circularity Z-score=0.9). Samples in Cluster C (Units 3, 4, and 5) can be most succinctly described as having more quartz than other samples in other clusters (percent quartz =0.9). Cluster D (1061-D3, Unit 2) is very different from the other clusters as it has the largest Z-scores. This sample has low variability in rounding and high variability in circularity with high ice contents (sd roundness=-3.8, sd circularity=3.2, and percent

ice=2.2). Lastly Cluster E (Unit 1) Z-scores indicate these samples are at a greater depth

and have less quartz on average (depth=1.2, percent quartz=-1).

2.5 Discussion

The combination of geochemical, mineralogical, and physical data collected from

the Camp Century sub-glacial materials across different spatial scales characterizes in

detail the 5 distinct stratigraphic units first defined by Bierman et al. (2024). From these

data, we infer that different surface processes deposited these materials during times

when the site was glaciated and when it was not. The rich record of ice sheet history and

process we interpret from these materials indicates that analysis of the geologic material

in sub-glacial cores can provide unique insight into past conditions extending deeper in

time than records preserved in the glacial ice above. Expanding paleoenvironmental

understanding of Greenland and its ice provides data to understand how both will behave

in a warmer future (Gemery & López-Quirós, 2024).

2.5.1 Sub-glacial Core Stratigraphy: Synthesis of Physical, Chemical, and Mineralogic Observations

Based on μCT scans, Unit 1 samples vary minimally, comprising a homogeneous

diamicton that we interpret as basal till. The sub-horizontal, braided, lenticular

cryostructures are consistent with syngenetic permafrost formation, suggesting on the

basis of cryostratigraphy, little influence of liquid water in Unit 1 after permafrost

formation (French & Shur, 2010). However. compared to other units, Unit 1 has more

abundant grain coatings (Fig. 5b), which are formed from percolating liquid water

(Marschalek et al., 2024). Warm conditions facilitated the accumulation of grain coatings

in the sediment before conditions supported the formation of permafrost and eventual burial by ice, after which the grain coatings have been preserved.

The high ice content at the top of Unit 3, and cryostructures suggesting epigenetic permafrost formation imply that the slumping occurring in the presence of liquid water, created a flow till deposit (Brevik & Reid, 2000). The mechanism causing slumping is unclear, it could be due to undercutting from a small stream or erosion of permafrost polygons. The normal grading seen in Unit 3 likely resulted from sorting as the sediments flowed downward, a sorting seen in flow till deposits (Brevik & Reid, 2000). The top of Unit 3 differs from the lower portion as there is distinct layering and an absence of large clasts. The layering in sample 1060-C2 and under the contact in 1060-C1 could be a marker of multiple flows (Fig. 2b). The lack of coarse clasts in the upper part of unit 3 may reflect limited flow capacity capable of moving only smaller particles during these subsequent flow events (Brevik & Reid, 2000). The paucity of grain coatings in Unit 3 compared to Unit 1 (Fig. 5), could indicate that the slumping process disrupted grain coatings or mixed sediment from Unit 1 with sediment from the upper units 4 and 5.

Unit 1, glacial till, and Unit 3, a slump deposit, have some similar characteristics in the μCT scans and similar mineralogy (Fig. 2). These similarities are seen in sample 1060-C3, the bottom of Unit 3, which is characterized by variably sized clasts in a fine-grained matrix with no evidence of bedding. The higher ice content and the difference in cryostructures between Units 1 and 3 supports the hypothesis that Unit 3 was deposited in or by liquid water. The presence of pyroxene in both units 1 and 3 links them beyond the meso-scale CT observations. Pyroxenes readily weather from sediments (Goldich, 1938)

so their inclusion in a sediment with high quartz content could reflect the source rock composition, limited weathering, or mixing with localized sources. Overall, the similar sedimentary structures and mineralogy indicate that Unit 3 was originally a part of the subglacial till formed below the ice (Unit 1) that was subject to slumping due to saturation of liquid water during interglacial conditions.

Unit 2, between Units 1 and 3, marks a stark transition from the sediment-dominated till to an ice matrix with interspersed sediments. The sediment content in Unit 2 and the horizontal alignment of grains in the ice is typical of a basal ice layer (Knight, 1997). The origin of the sediment interspersed in the ice is likely the till below (Unit 1) because they share similar geochemistry (presence of pyroxene) and fine particle aggregates, possibly glacial flour (Gresina et al., 2023; Knight, 1997). If Unit 2 were basal ice from the same advance that deposited Unit 1, then this ice would have survived for thousands of years after glacial retreat based on the calculations of Christ et. al (2023). Other origins of Unit 2 include interglacial firn or basal ice from a subsequent ice advance, a hypothesis that allows for deep weathering of Unit 1 (Hambreky et al., 1999).

In Units 4 and 5, there are high levels of sorting, minimal grain coatings, and the presence of bedding and contacts indicative of a fluvial depositional environment (Fig. 2). The fluvial system initially transported very fine-grained sands (Unit 4) followed by larger grains representing an increase in system energy (Unit 5). Grain morphology in these units is a mix of round and angular grains, with minimal change from Units 4 to 5 (Fig. 4), indicating the increase in system energy did not influence grain rounding (Kuenen, 1959).. Unique to Units 4 and 5, there are grains with coating in cracks or

concave structures that protected the coatings from abrasion during transport, preserving evidence of past weathering (Fig. 5). This implies that these sediments originally had more substantial grain coatings that were stripped during fluvial transport – consistent with geochronologic data indicating that minerals in Unit 1 and Unit 5 were similarly sourced (Christ et al., 2023)

The lack of the heavy minerals in the fluvial sediments could reflect hydraulic sorting, with the result that denser minerals, including pyroxene and amphibole, are deposited with larger grain size fractions (Malusà et al., 2016). This would explain the lack of heavy minerals in the finer grain size fraction (Unit 4) and the presence of amphibole at the top of Unit 5 where coarser grain sizes are included, brought in by a flow with the capacity to carry larger and denser grains (Garzanti, 2017; Malusà et al., 2016).

The PCA and K-means analysis informs our understanding of these transport processes and corroborates our hypotheses (Fig. 6). PC1, relating to transport processes, seems to separate the data between what could be considered glacially influenced (Units 1 and 2) and fluvially driven processes (Units 3, 4, and 5). Unit 3 samples overlap with Cluster E (Unit 1) which may be an indicator that supports our interpretation that these two units both originate from the same glacial till. PC2, relating to grain morphology, does not show any distinct trends relating to our unit assignments (Fig. 6). The grain morphology analysis exhibits a similar complexity (Fig. 4) which indicates intra-unit variability not seen on the meso or macro-scale.

Amongst all the units, Unit 2 is the most scattered across the PCA which could be an indication of a more complex history of formation for the ice unit. The SEM data for Unit 2 echoes this complexity as it has the most intra-unit variability. Despite the variation within the unit, some of the samples closely resemble other units at the micro-scale. Sample 1060-C4, at the top of Unit 2, is most reminiscent of an upper fluvial sample (Unit 5) as it has minimal grain coating and above-average grain size (Fig 6c). Conversely, sample 1061-B, near the middle of Unit 2, has aluminum-rich clay coatings which are also present in samples from Unit 3. On the PCA, 1061-B samples are situated in close proximity to Unit 1 and 3 samples, corroborating the similarities observed at the micro-scale. Samples closer to the contact with Unit 1 (1061-D3) are characterized by small particle aggregates that are unique to this section of core. The 1061-D3 samples plot at extreme ends of the PCA emphasizing their distinction from other parts of the core (Fig 6b).

The spread of data from Unit 2 could be an indication of environmental changes represented by this ice unit or of mixing between units above and below. For example, we have characterized Units 5 and 3 as having very different transport mechanisms and diagnostic characteristics of both these units are present in Unit 2. The inclusion of particles with characteristics similar to other units could imply that the changes seen throughout Unit 2 indicate variability in the mechanism of particle inclusion in the ice.

2.5.2 Proposed Sequence of Environmental Change at Camp Century

The Camp Century sub-glacial materials preserve changing surface and subglacial processes. From our multi-scale investigation of these materials, we present a plausible sequence of ice retreat and advance events consistent with evidence including surface exposure during MIS 11 (Fig. 7) (Christ et al., 2023).

1. *Initial conditions*: The bottom portion of the core (Unit 1) was subject to chemical weathering and experienced glacial transport. Glaciation in NW Greenland abraded the materials beneath the ice creating the basal till including cobble-sized clasts and fine rock flour.

2. *Retreat*: Ice then retreated exposing NW Greenland to surface processes, including the effect of moving water (Christ et al., 2021, 2023). This retreat may have left behind basal ice or Unit 2 may represent preserved snow/firn retained during interglacial times.

3. *Wet and Vegetated*: As interglacial conditions persisted, a permafrost landscape formed and was subject to freeze-thaw cycles as evidenced by the vertical lenses of clear ice in Unit 2. Till, saturated by water, flowed downslope and buried the ice forming Unit 3. Interglacial conditions then persisted, supporting plant growth and the development of a small fluvial system that the unconformable contact indicates eroded the upper portion of the flow-till deposit. The fluvial system then deposited bedded sand, initially fine-grained and then coarser-grained material.

4. *Readvance*: When the climate cooled after MIS 11, ice covered the Camp Century core site. This ice is currently cold-based and non-erosive.
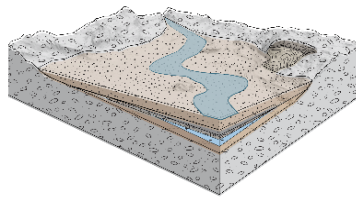
Unit 5 (MIS 11, 416 ± 38 ka)

Scale	Diagnostic features	Interpretation
Micro	84% of grains have little to no coating, wide distribution of grain sizes, 38.8% fine grained particles.	The fluvial system increases in energy enough to transport larger grain size sediment.
Meso	bedded sands, increasing in grain size toward top of unit	
Macro	39% quartz, 44% potassium feldspar, 17% plagioclase, <1% amphibole (only at the top of the unit)	
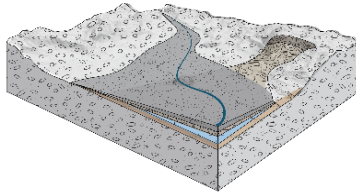
Unit 4

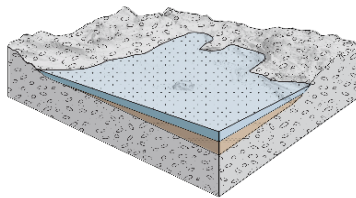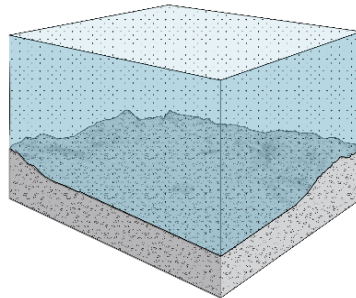| Scale	Diagnostic features	Interpretation
Micro	77% of grains have little to no coating, 59% fine grained fraction, very well sorted	Low energy fluvial system deposits well-sorted fine sand over slumped till (unit 3)
Meso	fine sand with well-defined parallel sub-horizontal bedding	
Macro	74% quartz, 21% plagioclase, 5% feldspar	

Unit 3

Scale	Diagnostic features	Interpretation
Micro	14% of grains have substantial coatings, samples lower in unit have more coatings, 40% fine grained particles	Interglacial conditions. The presence of liquid causes the upper portion of the subglacial till to slump over the remaining ice (unit 2), creating a flow till deposit with normal grading.
Meso	upper samples have high ice content with near vertical bedding, larger grains in the lower portion where bedforms are not visible	
Macro	66% quartz, 18% plagioclase, 10% feldspar, 6% pyroxene	

Unit 2

Scale	Diagnostic features	Interpretation
Micro	56% of grains have substantial coating, 78% fine-grained particles	Sediment laden ice (basal ice or firn) that survived interglacial conditions. Freeze-thaw cycles caused vertical fractures that filled with water that refroze.
Meso	>80% ice content with disseminated particles arranged in sub-horizontal bands, vertical fractures of clear ice	
Macro	75% quartz, 18% plagioclase, 7% potassium feldspar	

Unit 1 (>1.4 to <3.2 ± 0.4 Ma)

Scale	Diagnostic features	Interpretation
Micro	63% of grains have substantial coating, 46% fine-grained particles	Subglacial till weathered in place and resulting from prior glaciation that eroded the landscape
Meso	poor sorting, sub-horizontal ice lenses, matrix supported, no clear bedding	
Macro	57% quartz, 22% plagioclase, 12% potassium feldspar, 6% pyroxene, <2% Clay	

Figure 7. *Proposed sequence of events that led to the accumulation of the 5 units. Diagnostic features summarized by scale of observation. Time constraints based on past work (Christ et al., 2021, 2023).*

2.5.3 Implications

Multiscale investigation of the Camp Century sub-glacial materials documents glacial and deglacial processes on Greenland's surface over time. Systematic use of CT scanning has enhanced our ability to describe the sequence of environmental history stored in the basal material. Such meso-scale observations have led to the identification of transitions in environmental conditions, allowed us to observe internal sedimentary and cryogenic structures, and provide an archive of 3D models of the samples which no longer exist in their original state. Macro-scale XRD observations imply consistent sourcing of material. Micro-scale data allows linkages of process-specific attributes to the meso-scale observations. Uncertainties remain regarding the explanation for intra-unit variability, the extent and duration of ice-free conditions, and the history of formation for Unit 2. Further investigation into the Camp Century subglacial materials and other future collections of sub-glacial materials will refine the understanding of Greenland's paleoclimate and glaciologic history.

CHAPTER 3: CONCLUSION

In this work I have utilized sub-glacial materials to make interpretations of past environmental conditions on Greenland. I used multi-scale techniques to gather evidence of specific depositional processes both during glacial and deglacial times at the Camp Century site. This work is in collaboration with a large team of universities, faculty and students across the United States and Europe all focused on gaining surface process and climate insights from the 3.44 meters of sub-glacial materials. The data from this investigation will operate as a framework for future studies on the same material by providing environmental context for each sample of the core. Future studies will build on this work, enriching our understanding of the information stored in this material and eventually foster a better understanding of the future of the GrIS in a warming world.

Reflecting on this study, there are things I would do differently if I had the chance to do it over. The most powerful yet difficult part of the study was working with the CT scans. Some of this frustration could have been resolved if I had more preparation before traveling to CRREL or more guidance from an expert in CT scanning of sediments during our scan collection. This lack of preparation and guidance resulted in scans that could have been of higher quality, discrepancies between overlapping sections of the same sample, and overexposure of some samples which made quantitative analysis more difficult. I think more direction with how to quantify the suspended particles and material types would have led to more powerful usage of the data by allowing for fabric analysis, clast orientation evaluation, and identification and quantification of organic material in

the core. Despite the difficulties, the scans have still been greatly useful for meso-scale qualitative data that has enhanced the study greatly.

Another aspect I would wish to improve is the sampling resolution the core. Improving this resolution would be most useful in the transitional samples as I have had to lump the transitions in with just one unit which does not represent the data in the best way possible. 1060-C1 is an example where there are sediments from both Unit 3 and 4 but I only had access to combined bulk sediment from the entirety of the sample. It would be interesting to perform SEM analysis at the transition to see if there was a marker of change between the two units.

Overall, this research opportunity has been greatly enriching to me as a scientist as it has given me the opportunity to work on an international project working with very unique and historical material. The opportunity to work in a field that I find impactful considering today's climate concerns is motivating and I hope to continue to do such work in the future.

REFERENCES

Anderberg, M. R. (1973). *Cluster Analysis for Applications*. Elsevier.
https://doi.org/10.1016/C2013-0-06161-0

Bader, H. (1962). Scope, Problems, and Potential Value of Deep Core Drilling in Ice
Sheets. *CRREL Special Report 58*, 1–17.

Balter-Kennedy, A., Schaefer, J. M., Briner, J. P., Young, N. E., Walcott, C., Kuhl, T.,
Moravec, E., Keisling, B. A., Anandakrishnan, S., Stevens, N., & Brown, N. (2023).
First Results from GreenDrill: Exposure dating in sub-ice material from Prudhoe
Dome, northwestern Greenland. *(C14A-07) Presented at AGU23*.

Bender, M. L., Burgess, E., Alley, R. B., Barnett, B., & Clow, G. D. (2010). On the
nature of the dirty ice at the bottom of the GISP2 ice core. *Earth and Planetary
Science Letters*, *299*(3–4), 466–473. https://doi.org/10.1016/J.EPSL.2010.09.033

Bierman, P. R., Christ, A. J., Collins, C. M., Mastro, H. M., Souza, J., Blard, P.-H.,
Brachfeld, S., Courville, Z. R., Rittenour, T. M., Thomas, E. K., Tison, J.-L., &
Fripiat, F. (2024). Scientific history, sampling approach, and physical
characterization of the Camp Century sub-glacial sediment core, a rare archive from
beneath the Greenland Ice Sheet [Manuscript under review]. *The Cryosphere*.

Bierman, P. R., Corbett, L. B., Graly, J. A., Neumann, T. A., Lini, A., Crosby, B. T., &
Rood, D. H. (2014). Preservation of a Preglacial Landscape Under the Center of the
Greenland Ice Sheet. *Science*, *344*(6182), 402–405.
https://doi.org/10.1126/science.1249047

Bierman, P. R., Shakun, J. D., Corbett, L. B., Zimmerman, S. R., & Rood, D. H. (2016).
A persistent and dynamic East Greenland Ice Sheet over the past 7.5 million years.
Nature, *540*(7632), 256–260. https://doi.org/10.1038/nature20147

Bierman, P. R., Steig, E. J., Mastro, H. M., Corbett, L., Caffee, M., Hidy, Alan., &
Halsted, C. (2023). Fossil vegetation and 26Al/10Be in basal till from GISP2 core
further constrain existing interpretations of ice sheet history in central Greenland.
American Geophysical Union Fall Meeting., *C11D-1068*.

Blard, P. H., Protin, M., Tison, J. L., Fripiat, F., Dahl-Jensen, D., Steffensen, J. P.,
Mahaney, W. C., Bierman, P. R., Christ, A. J., Corbett, L. B., Debaille, V.,
Rigaudier, T., & Claeys, P. (2023). Basal debris of the NEEM ice core, Greenland: a
window into sub-ice-sheet geology, basal ice processes and ice-sheet oscillations.
Journal of Glaciology, *268*(11). https://doi.org/10.1017/jog.2022.122

Bond, G., Heinrich, H., Broecker, W., Labeyrie, L., McManus, J., Andrews, J., Huon, S.,
Jantschik, R., Clasen, S., Simet, C., Tedesco, K., Klas, M., Bonani, G., & Ivy, S.
(1992). Evidence for massive discharges of icebergs into the North Atlantic ocean
during the last glacial period. *Nature*, *360*(6401), 245–249.
https://doi.org/10.1038/360245a0

Box, J. E., Hubbard, A., Bahr, D. B., Colgan, W. T., Fettweis, X., Mankoff, K. D.,
Wehrlé, A., Noël, B., van den Broeke, M. R., Wouters, B., Bjørk, A. A., & Fausto,
R. S. (2022). Greenland ice sheet climate disequilibrium and committed sea-level
rise. *Nature Climate Change*, *12*(9), 808–813. https://doi.org/10.1038/s41558-022-
01441-2

Brevik, E. C., & Reid, J. R. (2000). Differentiating Till and Debris Flow Deposits in Glacial Landscapes. *Soil Horizons*, *41*(3), 83. https://doi.org/10.2136/sh2000.3.0083

Briner, J. P., Walcott, C. K., Schaefer, J. M., Young, N. E., MacGregor, J. A., Poinar, K., Keisling, B. A., Anandakrishnan, S., Albert, M. R., Kuhl, T., & Boeckmann, G. (2022). Drill-site selection for cosmogenic-nuclide exposure dating of the bed of the Greenland Ice Sheet. *The Cryosphere*, *16*(10), 3933–3948. https://doi.org/10.5194/tc-16-3933-2022

Calmels, F., & Allard, M. (2008). Segregated Ice Structures in Various Heaved Permafrost Landforms Through CT Scan. *Earth Surf. Process. Landforms*, *33*, 209–225. https://doi.org/10.1002/esp

Christ, A. J., Bierman, P. R., Schaefer, J. M., Dahl-Jensen, D., Steffensen, J. P., Corbett, L. B., Peteet, D. M., Thomas, E. K., Steig, E. J., Rittenour, T. M., Tison, J.-L., Blard, P.-H., Perdrial, N., Dethier, D. P., Lini, A., Hidy, A. J., Caffee, M. W., & Southon, J. (2021). A multimillion-year-old record of Greenland vegetation and glacial history preserved in sediment beneath 1.4 km of ice at Camp Century. *PNAS*, *118*(13). https://doi.org/10.1073/pnas.2021442118/-/DCSupplemental

Christ, A. J., Rittenour, T. M., Bierman, P. R., Keisling, B. A., Knutz, P. C., Thomsen, T. B., Keulen, N., Fosdick, J. C., Hemming, S. R., Tison, J.-L., Blard, P.-H., Steffensen, J. P., Caffee, M. W., Corbett, L. B., Dahl-Jensen, D., Dethier, D. P., Hidy, A. J., Perdrial, N., Peteet, D. M., … Thomas, E. K. (2023). Deglaciation of northwestern Greenland during Marine Isotope Stage 11. *Science*, *381*(6655), 330–335. https://doi.org/10.1126/science.ade4248

Clark, E. F. (1965). *Camp Century Evolution of Concept and History of Design Construction and Performance*.

de Vernal, A., & Hillaire-Marcel, C. (2008). Natural Variability of Greenland Climate, Vegetation, and Ice Volume During the Past Million Years. *Science*, *320*(5883), 1622–1625. https://doi.org/10.1126/science.1153929

Dixon, J. C., Thorn, C. E., Darmody, R. G., & Campbell, S. W. (2002). Weathering rinds and rock coatings from an Arctic alpine environment, northern Scandinavia. *Geological Society of America Bulletin*, *114*(2), 226–238. https://doi.org/10.1130/0016-7606(2002)114<0226:WRARCF>2.0.CO;2

Dutton, A., Carlson, A. E., Long, A. J., Milne, G. A., Clark, P. U., DeConto, R., Horton, B. P., Rahmstorf, S., & Raymo, M. E. (2015). Sea-level rise due to polar ice-sheet mass loss during past warm periods. *Science*, *349*(6244). https://doi.org/10.1126/science.aaa4019

Emmanouilidis, A., Messaris, G., Ntzanis, E., Zampakis, P., Prevedouros, I., Bassukas, D. A., & Avramidis, P. (2020). CT scanning, X-ray fluorescence: Non-destructive techniques for the identification of sedimentary facies and structures. *Revue de Micropaleontologie*, *67*. https://doi.org/10.1016/j.revmic.2020.100410

Fountain, J., Usselman, T. M., Wooden, J., & Langway, C. C. (1981). Evidence of the Bedrock Beneath the Greenland Ice Sheet Near Camp Century, Greenland. *Journal of Glaciology*, *27*(95), 193–197. https://doi.org/10.3189/S0022143000011370

French, H., & Shur, Y. (2010). The principles of cryostratigraphy. *Earth-Science Reviews*, *101*(3–4), 190–206. https://doi.org/10.1016/j.earscirev.2010.04.002

Garzanti, E. (2017). The Maturity Myth In Sedimentology and Provenance Analysis. *Journal of Sedimentary Research*, *87*(4), 353–365. https://doi.org/10.2110/jsr.2017.17

Gemery, L., & López-Quirós, A. (2024). Polar paleoenvironmental perspectives on modern climate change. *PLOS Climate*, *3*(1), e0000333. https://doi.org/10.1371/journal.pclm.0000333

Goldich, S. S. (1938). A Study in Rock-Weathering. *The Journal of Geology*, *46*(1), 17–58. https://doi.org/10.1086/624619

Gow, A. J., & Meese, D. A. (1996). Nature of basal debris in the GISP2 and Byrd ice cores and its relevance to bed processes. *Annals of Glaciology*, *22*, 134–140. https://doi.org/10.3189/1996AoG22-1-134-140

Gow, A. J., Meese, D. A., Alley, R. B., Fitzpatrick, J. J., Anandakrishnan, S., Woods, G. A., & Elder, B. C. (1997). Physical and structural properties of the Greenland Ice Sheet Project 2 ice core: A review. *Journal of Geophysical Research: Oceans*, *102*(C12), 26559–26575. https://doi.org/10.1029/97JC00165

Gresina, F., Farkas, B., Fábián, S. Á., Szalai, Z., & Varga, G. (2023). Morphological analysis of mineral grains from different sedimentary environments using automated static image analysis. *Sedimentary Geology*, *455*, 106479. https://doi.org/10.1016/j.sedgeo.2023.106479

Grousset, F. E., Labeyrie, L., Sinko, J. A., Cremer, M., Bond, G., Duprat, J., Cortijo, E., & Huon, S. (1993). Patterns of Ice-Rafted Detritus in the Glacial North Atlantic (40-55°N). *Paleoceanography*, *8*(2), 175–192. https://doi.org/10.1029/92PA02923

Hambreky, M. J., Bennett, M. R., Dowdeswell, J. A., Glasser, N. F., & Huddart, D. (1999). Debris entrainment and transfer in polythermal valley glaciers. *Journal of Glaciology*, *45*(149), 69–86. https://doi.org/10.3189/S0022143000003051

Hansen, B. L., & Langway, C. C. (1966a). Deep Core Drilling in Ice and Core Analysis at Camp Century, Greenland, 1961-1966. *Antarctic Journal of the United States*, *1*(5), 207–208.

Hansen, B. L., & Langway, C. C. (1966b). *Glaciology Deep Core Drilling in Ice and Core Analysis at Camp Century, Greenland, 1961-1966*.

Harwood, D. M. (1986). Do Diatoms beneath the Greenland Ice Sheet Indicate Interglacials Warmer than Present? *Arctic*, *39*(4), 304–308.

Herron, S., Hoar, & Langway, C. C. (1979). The Debris-Laden Ice at the Bottom of the Greenland Ice Sheet. *Journal of Glaciology*, *23*(89), 193–207. https://doi.org/10.3189/s002214300002983x

Hjulström, F. (1935). *Studies of the morphological activity of rivers as illustrated by the River Fyris*. Uppsala University.

Janoo, V. C. (1998). Quantification of Shape, Angularity, and Surface texture of Base Course Materials. *US Transportation Collection*.

Jansson, N. F., Allen, R. L., Skogsmo, G., & Tavakoli, S. (2022). Principal component analysis and K-means clustering as tools during exploration for Zn skarn deposits and industrial carbonates, Sala area, Sweden. *Journal of Geochemical Exploration*, *233*, 106909. https://doi.org/10.1016/j.gexplo.2021.106909

JMP (Version 18.0). (2024). SAS Institute Inc.

Johnsen, S. J., Dahl-Jensen, D., Gundestrup, N., Steffensen, J. P., Clausen, H. B., Miller, H., Masson-Delmotte, V., Sveinbjörnsdottir, A. E., & White, J. (2001). Oxygen isotope and palaeotemperature records from six Greenland ice-core stations: Camp Century, Dye-3, GRIP, GISP2, Renland and NorthGRIP. *Journal of Quaternary Science*, *16*(4), 299–307. https://doi.org/10.1002/JQS.622

Johnsen, S. J., Dansgaard, W., Clausen, H. B., & Lang Way, C. C. (1972). Oxygen Isotope Profiles through the Antarctic and Greenland Ice Sheets. In *Biochem. Biophys. Res. Commun* (Vol. 235).

Jouzel, J., Masson-Delmotte, V., Cattani, O., Dreyfus, G., Falourd, S., Hoffmann, G., Minster, B., Nouet, J., Barnola, J. M., Chappellaz, J., Fischer, H., Gallet, J. C., Johnsen, S., Leuenberger, M., Loulergue, L., Luethi, D., Oerter, H., Parrenin, F., Raisbeck, G., … Wolff, E. W. (2007). Orbital and Millennial Antarctic Climate Variability over the Past 800,000 Years. *Science*, *317*(5839), 793–796. https://doi.org/10.1126/science.1141038

Kalińska-Nartiša, E., Stivrins, N., & Grudzinska, I. (2018). Quartz grains reveal sedimentary palaeoenvironment and past storm events: A case study from eastern Baltic. *Estuarine, Coastal and Shelf Science*, *200*, 359–370. https://doi.org/10.1016/j.ecss.2017.11.027

Keulen, N., Malkki, S. N., & Graham, S. (2020). Automated Quantitative Mineralogy Applied to Metamorphic Rocks. *Minerals*, *10*(1), 47. https://doi.org/10.3390/min10010047

Knight, P. G. (1997). The basal ice layer of glaciers and ice sheets. *Quaternary Science Reviews*, *16*(9), 975–993. https://doi.org/10.1016/S0277-3791(97)00033-4

Krumbein, W. C. (1941). The Effects of Abrasion on the Size, Shape and Roundness of Rock Fragments. *The Journal of Geology*, *49*(5), 482–520. https://doi.org/10.1086/624985

Kuenen, P. H. (1959). Experimental abrasion; 3, Fluviatile action on sand. *American Journal of Science*, *257*(3), 172–190. https://doi.org/10.2475/ajs.257.3.172

Kukla, G., McManus, J. F., Rousseau, D. D., & Chuine, I. (1997). How long and how stable was the last interglacial? *Quaternary Science Reviews*, *16*(6), 605–612. https://doi.org/10.1016/S0277-3791(96)00114-X

Langway, C. C. (2008). The History of Early Polar Ice Cores. *Cold Regions Science and Technology*, *52*(2), 101–117. https://doi.org/10.1016/j.coldregions.2008.01.001.

Langway, C. C., & Hansen, B. L. (1970). Drilling Through the Ice Cap: Probing Climate for a Thousand Centuries. *Bulletin of the Atomic Scientists*, *26*(10), 62–66.

Lapalme, C. M., Lacelle, D., Pollard, W., Fortier, D., Davila, A., & McKay, C. P. (2017). Cryostratigraphy and the Sublimation Unconformity in Permafrost from an Ultraxerous Environment, University Valley, McMurdo Dry Valleys of Antarctica. *Permafrost and Periglacial Processes*, *28*(4), 649–662. https://doi.org/10.1002/ppp.1948

Lee, A. S., Enters, D., Titschack, J., & Zolitschka, B. (2021). Facies characterisation of sediments from the East Frisian Wadden Sea (Germany): New insights from down-core scanning techniques. *Geologie En Mijnbouw/Netherlands Journal of Geosciences*. https://doi.org/10.1017/njg.2021.6

Lei, L., Park, T., Jarvis, K., Pan, L., Tepecik, I., Zhao, Y., Ge, Z., Choi, J.-H., Gai, X., Galindo-Torres, S. A., Boswell, R., Dai, S., & Seol, Y. (2022). Pore-scale observations of natural hydrate-bearing sediments via pressure core sub-coring and micro-CT scanning. *Scientific Reports*, *12*(1), 3471. https://doi.org/10.1038/s41598-022-07184-6

Lei, L., Seol, Y., & Jarvis, K. (2018). Pore-Scale Visualization of Methane Hydrate-Bearing Sediments With Micro-CT. *Geophysical Research Letters*, *45*(11), 5417–5426. https://doi.org/10.1029/2018GL078507

Lisiecki, L. E., & Raymo, M. E. (2005). A Pliocene-Pleistocene stack of 57 globally distributed benthic δ18O records. *Paleoceanography*, *20*(1), 1–17. https://doi.org/10.1029/2004PA001071

Loutre, M. F., & Berger, A. (2003). Marine Isotope Stage 11 as an analogue for the present interglacial. *Global and Planetary Change*, *36*(3), 209–217. https://doi.org/10.1016/S0921-8181(02)00186-8

Lüthi, D., Le Floch, M., Bereiter, B., Blunier, T., Barnola, J.-M., Siegenthaler, U., Raynaud, D., Jouzel, J., Fischer, H., Kawamura, K., & Stocker, T. F. (2008). High-resolution carbon dioxide concentration record 650,000–800,000 years before present. *Nature*, *453*(7193), 379–382. https://doi.org/10.1038/nature06949

Mackowiak, T. J., & Perdrial, N. (2023). Monitoring of Suspended Sediment Mineralogy in Puerto-Rican Rivers: Effects of Flowrate and Lithology. *Minerals*, *13*(2), 208. https://doi.org/10.3390/min13020208

Malusà, M. G., Resentini, A., & Garzanti, E. (2016). Hydraulic sorting and mineral fertility bias in detrital geochronology. *Gondwana Research*, *31*, 1–19. https://doi.org/10.1016/j.gr.2015.09.002

Manabe, S., & Stouffer, R. J. (1980). Sensitivity of a global climate model to an increase of CO2 concentration in the atmosphere. *Journal of Geophysical Research*, *85*(C10), 5529. https://doi.org/10.1029/JC085iC10p05529

Marschalek, J. W., Blard, P. -H., Sarigulyan, E., Ehrmann, W., Hemming, S. R., Thomson, S. N., Hillenbrand, C. -D., Licht, K., Tison, J. -L., Ardoin, L., Fripiat, F., Allen, C. S., Marrocchi, Y., Siegert, M. J., & van de Flierdt, T. (2024). Byrd Ice Core Debris Constrains the Sediment Provenance Signature of Central West Antarctica. *Geophysical Research Letters*, *51*(5). https://doi.org/10.1029/2023GL106958

Mena, A., Francés, G., Pérez-Arlucea, M., Aguiar, P., Barreiro-Vázquez, J. D., Iglesias, A., & Barreiro-Lois, A. (2015). A novel sedimentological method based on CT-scanning: Use for tomographic characterization of the Galicia Interior Basin. *Sedimentary Geology*, *321*, 123–138. https://doi.org/10.1016/j.sedgeo.2015.03.007

Murton, J. B., & French, H. M. (1994). Cryostructures in permafrost, Tuktoyaktuk coastlands, western arctic Canada. *Canadian Journal of Earth Sciences*, *31*(4), 737–747. https://doi.org/10.1139/e94-067

Musselman, Z. A., & Tarbox, A. M. (2013). Downstream Trends in Grain Size, Angularity, and Sorting of Channel-Bed and Bank Deposits in a Coastal Plain Sand-Bed River: the Pascagoula River System, Mississippi, USA. *Southeastern Geographer*, *53*(2), 177–197. https://doi.org/10.1353/sgo.2013.0017

Naqshband, S., & McElroy, B. (2016). Sediment transport at grain scale: A review, future research and morphological implications. *River Flow 2016*, 914–918. https://doi.org/10.1201/9781315644479-145

Nitzbon, J., Gadylyaev, D., Schlüter, S., Köhne, J. M., Grosse, G., & Boike, J. (2022). Brief communication: Unravelling the composition and microstructure of a permafrost core using X-ray computed tomography. *The Cryosphere*, *16*(9), 3507–3515. https://doi.org/10.5194/tc-16-3507-2022

Orsi, T. H., Edwards, C. M., & Anderson', A. L. (1994). X-Ray Computed Tomography: A Non-destructive Method for Quantitative Analysis of Sediment Cores. *Journal of Sedimentary Research*, *64A*(3), 690–693. http://pubs.geoscienceworld.org/sepm/jsedres/article-pdf/64/3a/690/2812031/690.pdf

Pesch, C., Weber, P. L., Moldrup, P., de Jonge, L. W., Arthur, E., & Greve, M. H. (2022). Physical characterization of glacial rock flours from fjord deposits in South Greenland–Toward soil amendment. *Soil Science Society of America Journal*, *86*(2), 407–422. https://doi.org/10.1002/saj2.20352

Preibisch, S., Saalfeld, S., & Tomancak, P. (2009). Globally optimal stitching of tiled 3D microscopic image acquisitions. *Bioinformatics*, *25*(11), 1463–1465. https://doi.org/10.1093/bioinformatics/btp184

R Core Team. (2022). *R: A Language and Environment for Statistical Computing* (4.2.2). R Foundation for Statistical Computing.

Rantanen, M., Karpechko, A. Yu., Lipponen, A., Nordling, K., Hyvärinen, O., Ruosteenoja, K., Vihma, T., & Laaksonen, A. (2022). The Arctic has warmed nearly four times faster than the globe since 1979. *Communications Earth & Environment*, *3*(1), 168. https://doi.org/10.1038/s43247-022-00498-3

Razi, T., Niknami, M., & Alavi Ghazani, F. (2014). Relationship between Hounsfield Unit in CT Scan and Gray Scale in CBCT. *Journal of Dental Research, Dental Clinics, Dental Prospects*, *8*(2), 107–110. https://doi.org/10.5681/joddd.2014.019

Renter, J. A. M. (1989). Applications of computerized tomography in sedimentology. *Marine Geotechnology*, *8*(3), 201–211. https://doi.org/10.1080/10641198909379868

Rentschler, J., Salhab, M., & Jafino, B. A. (2022). Flood exposure and poverty in 188 countries. *Nature Communications*, *13*(1), 3527. https://doi.org/10.1038/s41467-022-30727-4

Reyes, A. V, Carlson, A. E., Beard, B. L., Hatfield, R. G., Stoner, J. S., Winsor, K., Welke, B., & Ullman, D. J. (2014a). South Greenland ice-sheet collapse during Marine Isotope Stage 11. *Nature*. https://doi.org/10.1038/nature13456

Reyes, A. V., Carlson, A. E., Beard, B. L., Hatfield, R. G., Stoner, J. S., Winsor, K., Welke, B., & Ullman, D. J. (2014b). South Greenland ice-sheet collapse during Marine Isotope Stage 11. *Nature*, *510*(7506), 525–528. https://doi.org/10.1038/nature13456

Rietveld, H. M. (1969). A profile refinement method for nuclear and magnetic structures. *Journal of Applied Crystallography*, *2*(2), 65–71. https://doi.org/10.1107/S0021889869006558

Schaefer, J. M., Finkel, R. C., Balco, G., Alley, R. B., Caffee, M. W., Briner, J. P., Young, N. E., Gow, A. J., & Schwartz, R. (2016). Greenland was nearly ice-free for extended periods during the Pleistocene. *Nature*, *540*(7632), 252–255. https://doi.org/10.1038/nature20146

Schindelin, J., Arganda-Carreras, I., Frise, E., Kaynig, V., Longair, M., Pietzsch, T., Preibisch, S., Rueden, C., Saalfeld, S., Schmid, B., Tinevez, J.-Y., White, D. J., Hartenstein, V., Eliceiri, K., Tomancak, P., & Cardona, A. (2012). Fiji: an open-source platform for biological-image analysis. *Nature Methods*, *9*(7), 676–682. https://doi.org/10.1038/nmeth.2019

Smith, B., Fricker, H. A., Gardner, A. S., Medley, B., Nilsson, J., Paolo, F. S., Holschuh, N., Adusumilli, S., Brunt, K., Csatho, B., Harbeck, K., Markus, T., Neumann, T., Siegfried, M. R., & Zwally, H. J. (2020). *Pervasive ice sheet mass loss reflects competing ocean and atmosphere processes*. https://doi.org/10.1126/science.aaz5845

Souchez, R., Bouzette, A., Clausen, H. B., Johnsen, S. J., & Jouzel, J. (1998). A stacked mixing sequence at the base of the Dye 3 core, Greenland. *Geophysical Research Letters*, *25*(10), 1943–1946. https://doi.org/10.1029/98gl01411

Souchez, R., Janssens, L., Lemmens, M., & Stauffer, B. (1995). Very low oxygen concentration in basal ice from Summit, central Greenland. *Geophysical Research Letters*, *22*(15), 2001–2004. https://doi.org/10.1029/95GL01995

Souchez, R., Tison, J. -L, Lorrain, R., Lemmens, M., Janssens, L., Stievenard, M., Jouzel, J., Sveinbjörnsdottir, A., & Johnsen, S. J. (1994). Stable isotopes in the basal silty ice preserved in the Greenland Ice Sheet at summit; environmental implications. *Geophysical Research Letters*, *21*(8), 693–696. https://doi.org/10.1029/94GL00641

Suwa, M., von Fischer, J. C., Bender, M. L., Landais, A., & Brook, E. J. (2006a). Chronology reconstruction for the disturbed bottom section of the GISP2 and the GRIP ice cores: Implications for Termination II in Greenland. *Journal of Geophysical Research: Atmospheres*, *111*(D2), 2101. https://doi.org/10.1029/2005JD006032

Suwa, M., von Fischer, J. C., Bender, M. L., Landais, A., & Brook, E. J. (2006b). Chronology reconstruction for the disturbed bottom section of the GISP2 and the GRIP ice cores: Implications for Termination II in Greenland. *Journal of Geophysical Research Atmospheres*, *111*(2). https://doi.org/10.1029/2005JD006032

Svensson, A., Bigler, M., Kettner, E., Dahl-Jensen, D., Johnsen, S., Kipfstuhl, S., Nielsen, M., & Steffensen, J. P. (2011). Annual layering in the NGRIP ice core during the Eemian. *Climate of the Past*, *7*(4), 1427–1437. https://doi.org/10.5194/CP-7-1427-2011

Szmańda, J. B., & Witkowski, K. (2021). Morphometric Parameters of Krumbein Grain Shape Charts—A Critical Approach in Light of the Automatic Grain Shape Image Analysis. *Minerals*, *11*(9), 937. https://doi.org/10.3390/min11090937

Tafesse, S., Robison Fernlund, J. M., Sun, W., & Bergholm, F. (2013). Evaluation of image analysis methods used for quantification of particle angularity. *Sedimentology*, *60*(4), 1100–1110. https://doi.org/10.1111/j.1365-3091.2012.01367.x

Tison, J., Thorsteinsson, T., & Lorrain, R. (1994). EPSL Origin and development of textures and fabrics in basal ice at Summit, Central Greenland. *Earth and Planetary Science Letters*, *125*, 421–437.

van Hateren, J. A., van Buuren, U., Arens, S. M., van Balen, R. T., & Prins, M. A. (2020). Identifying sediment transport mechanisms from grain size–shape distributions, applied to aeolian sediments. *Earth Surface Dynamics*, *8*(2), 527–553. https://doi.org/10.5194/esurf-8-527-2020

Vandel, E., Vaasma, T., & Sugita, S. (2020). Application of image analysis technique for measurement of sand grains in sediments. *MethodsX*, *7*, 100981. https://doi.org/10.1016/j.mex.2020.100981

Vandenberghe, J., & Nugteren, G. (2001). Rapid climatic changes recorded in loess successions. *Global and Planetary Change*, *28*(1–4), 1–9. https://doi.org/10.1016/S0921-8181(00)00060-6

Voosen, P. (2019). Mud in storied ice core hints at a thawed Greenland. *Science*, *366*(6465), 556–557. https://doi.org/10.1126/science.366.6465.556

W. Dansgaard, S. J. Johnsen, J. Moller, & C. C. Langway Jr. (1969). One Thousand Centuries of Climatic Record from Camp Century on the Greenland Ice Sheet. *Science*.

Whalley, W. B., & Langway, C. C. (1980). A Scanning Electron Microscope Examination of Subglacial Quartz Grains from Camp Century Core, Greenland–A Preliminary Study. *Journal of Glaciology*, *25*(91), 125–132. https://doi.org/10.3189/s0022143000010340

Willerslev, E., Cappellini, E., Boomsma, W., Nielsen, R., Hebsgaard, M. B., Brand, T. B., Hofreiter, M., Bunce, M., Poinar, H. N., Dahl-Jensen, D., Johnsen, S., Steffensen, J. P., Bennike, O., Schwenninger, J. L., Nathan, R., Armitage, S., De Hoog, C. J., Alfimov, V., Christl, M., … Collins, M. J. (2007). Ancient biomolecules from deep ice cores reveal a forested southern Greenland. *Science*, *317*(5834), 111–114. https://doi.org/10.1126/SCIENCE.1141758/SUPPL_FILE/WILLERSLEV.SOM.REVISION.1.PDF

Willerslev, E., Cappellini, E., Boomsma, W., Nielsen, R., Hebsgaard, M. B., Brand, T. B., Hofreiter, M., Bunce, M., Poinar, H. N., Dahl-Jensen, D., Johnsen, S., Steffensen, J. P., Bennike, O., Schwenninger, J.-L., Nathan, R., Armitage, S., de Hoog, C.-J., Alfimov, V., Christl, M., … Collins, M. J. (2007). Ancient Biomolecules from Deep Ice Cores Reveal a Forested Southern Greenland. *Science*, *317*(5834), 111–114. https://doi.org/10.1126/science.1141758

Woronko, B., Pisarska-Jamroży, M., & Loon, A. J. (Tom) van. (2015). Reconstruction of sediment provenance and transport processes from the surface textures of quartz grains from Late Pleistocene sandurs and an ice-marginal valley in NW Poland. *Geologos*, *21*(2), 105–115. https://doi.org/10.1515/logos-2015-0007

Yau, A. M., Bender, M. L., Blunier, T., & Jouzel, J. (2016). Setting a chronology for the basal ice at Dye-3 and GRIP: Implications for the long-term stability of the Greenland Ice Sheet. *Earth and Planetary Science Letters*, *451*, 1–9. https://doi.org/10.1016/J.EPSL.2016.06.053